IN-46
411354

Decadal Air-Sea Interaction in the North Atlantic based on observations and modeling results

Sirpa Häkkinen,

NASA Goddard Space Center, Code 971, Greenbelt MD 20771

September 1998

Submitted to Journal of Climate

Abstract.

The decadal, 12-14 year, cycle observed in the North Atlantic SST and tide gauge data was examined using the NCEP/NCAR reanalyses, COADS data and an ocean model simulation. Besides this decadal mode, a shorter, subdecadal period of about 8 years exists in tide gauge data north of 40N, in the subpolar SST and in the winter North Atlantic Oscillation (NAO) index and in subpolar winter heat flux values. The decadal cycle is a well separated mode in a singular spectrum analysis (SSA) for a time series of SST EOF mode 1 with a center over the Gulf Stream extension. Tide gauge and SST data are consistent in that both show a significant subdecadal periodicity exclusively in the subpolar gyre, but in subtropics the 12-14 year period is the prominent, but nonstationary, decadal signal. The main finding of this study is that this 12-14 year cycle can be constructed based on the leading mode of the surface heat flux. This connection to the surface heat flux implicates the participation of the thermohaline circulation in the decadal cycle. During the cycle starting from the positive index phase of NAO, SST and oceanic heat content anomalies are created in subtropics due to local heat flux and intensification of the thermohaline circulation. The anomalies advect to the subpolar gyre where they are amplified by local heat flux and are part of the negative feedback of thermohaline circulation on itself. Consequently the oceanic thermohaline circulation slows down and the opposite cycle starts. The oscillatory nature would not be possible without the active atmospheric participation in the cycle, because it provides the unstable interaction through heat flux, without it, the oceanic mode would be damped. This analysis suggests that the two principal modes of heat flux variability, corresponding to patterns similar to North Atlantic Oscillation (NAO) and Western Atlantic (WA), are part of the same decadal cycle and an indirect measure of the north-south movement of the storm tracks.

1. Introduction

The North Atlantic ocean and atmosphere exhibit apparent long term climate variations, some of which might arise from coupled interactions. Existence of such coupled modes could provide significant potential for climate predictability as exemplified by the most well known coupled phenomemon, El Nino, for which the atmosphere-ocean interactions are rather well understood (Neelin et al., 1998). However, the existence of mid-latitude coupled modes has been under debate for some time, because a definite process is yet to be singled out through which the coupled interactions would be acting; likely candidates being wind driven gyre dynamics and thermohaline circulation. At decadal and longer time scales the ocean dynamics and thermodynamics are expected to play a role in climate variability due to the oceanic memory (Bjerknes, 1964). Several studies on the decadal variability of N. Atlantic SST report an oscillatory mode of a period of 12-14 years (Deser and Blackmon 1993; Sutton and Allen 1997; Moron et al. 1998). A study by Unal and Ghil (1995) finds 10-13 year periodicity in sea level around the North Atlantic coasts. A sub-decadal mode is also evident in the wintertime NAO defined as the difference of sea level pressure between Icelandic low and Azorian high (Hurrell, 1995). This periodicity is also found in SST by Moron et al. (1998) and Mann and Park (1994). Mechanisms such as a local oceanic response to the atmospheric anomalies (Deser and Blackmon 1993; Battisti et al. 1995), and the advection of winter SST anomalies (SSTA) along the path of the North Atlantic Current (NAC) (Sutton and Allen 1997) have been suggested as key elements responsible for the decadal mode.

Coupled modeling can give insights to the longer term variability by providing long time series of dynamically consistent fields. The study by Grötzner et al. (1998) finds a decadal coupled mode in the North Atlantic with periodicity of about 17 years, dynamically similar to the one in the North Pacific (Latif and Barnett, 1994): The mode is maintained by wind driven changes in the gyre circulation which in turn create oceanic heat content variations in the Gulf Stream and its extension. The atmospheric response to the heat content changes in the subtropics change the wind stress curl causing a delayed negative feedback to gyre circulation. Even in a case without explicit existence of coupled modes, Saravanan and McWilliams (1998) suggest based on a simplified coupled model of

ocean and white noise atmosphere that the slow advection of SST anomalies associated with the North Atlantic thermohaline cell enhances the variability at decadal frequency. They demonstrate existence of orthogonal modes in the oceanic response which peak at the preferred frequency when advection and atmospheric damping of thermal anomalies are about similar strength. In their case the source of the decadal frequency is in thermal forcing, but some others (Weisse et al., 1994) have generated such oscillations using stochastic fresh water forcing in the subpolar gyre. Thus, the role of thermal versus haline stochastic forcing is less than clear. Considering the haline effects, the 12-14 year frequency is present in the regular appearance of salinity anomalies in the subpolar gyre (Reverdin et al 1997). These anomalies are also accompanied with sea ice and SST anomalies (Deser and Blackmon, 1993) although it has not been determined whether the sea ice was the cause or simply a passive tracer for the negative salinity anomalies.

The subject of this study is the ocean-atmosphere heat exchange and how it is connected to the decadal variations in the mid-latitude atmosphere-ocean system. Consideration of the surface heat flux leads to the question of the role of the thermohaline circulation in the decadal variability, which is the main focus of this study. In a model simulation for 1951-1993 of Häkkinen (1998), the meridional overturning cell (MOC) and heat transport (MHT) are shown to reflect predominantly, and to be driven by, the variability of the NAO related heat flux. The northern center of the NAO related heat flux located in the subpolar gyre controls the strength of convection (and thus MOC). The MOC changes are result of variations in the volume in the Labrador Sea Water (LSW), as the simulated Nordic Sills overflow did not vary significantly during the same period. MOC and MHT changes in the subtropics lag typically 2 years the NAO heat flux changes. This intensified MOC appears as anomalously high sea level height in the Gulf Stream-North Atlantic Current region as a result from an enhanced heat content of the ocean. The oceanic response occurs within one year from the maximum MHT at 25N. Thus, we can causally relate the leading heat flux mode to the strength of the overturning and heat content anomalies in the North Atlantic. As already anticipated in the study by Sutton and Allen (1997), these heat content anomalies due to the changes in MOC do occur in the storm formation area which is the Gulf Stream area. Another finding of interest for this work in Häkkinen (1998) is that

although the second mode of heat flux corresponding to a sea level pressure (SLP) pattern with the closest resemblance to the Western Atlantic (WA) pattern was not the driving force of the overturning, it appeared with equally high correlation with MHT. In fact, at higher latitudes (north of 40N) the peaks in MHT were leading the time series of the second heat flux mode, suggesting that strenghened overturning and heat content anomalies in the storm formation area modulate the low frequency variability of the second heat flux mode.

To view the recent 40 year variability in a long-term perspective, the historical data was first analyzed for decadal cycles. This data consists of SST reconstruction with 6x6 degree resolution by Smith et al. (1998) for period 1856-1997, and of tide gauges records, some spanning over 100 years, from The Permanent Service for Mean Sea Level (PMSL; at Bidston, UK). To study the variability during the recent 40 years we employ the NCEP/NCAR reanalysis (retrieved from the web-site of NOAA-CIRES Climate Diagnostics Center at Boulder, CO) for the period 1958-1997 and COADS data (1946-1993) by daSilva et al. (1994) and a model simulation for 1951-1993 which uses COADS anomalies. The SST data used in the reanalysis are from the EOF reconstructed SSTs for the period 1950-1997 (Smith et al. 1996). Sea level pressure (SLP) data was obtained from the NCAR 5x5 SLP data set for period 1946-1995. The ocean simulation is the same as discussed in Häkkinen (1998) for effects of NAO in meridional heat transport variability.

The model formulation and forcing are briefly discussed in Section 2. It will be shown that a decadal and a subdecadal mode exist in the oceanic SST and tide gauge data, but the former is of nonstationary nature in SST, Section 3.1. The observational analysis and model simulation data are compared and primary associations with leading heat flux patterns of NAO and WA are derived in Section 3.2. Section 4 shows that this decadal mode with a 12-14 year period is a coupled mode. In this mode the local oceanic response to atmospheric circulation off the N. American coast, the advection of SST and ocean heat content anomalies along the Gulf Stream/NAC and feedbacks from the oceanic heat content to the atmosphere all play a role.

2. Ocean model and surface forcing

The coupled ocean and ice model is previously published in Häkkinen and Mellor (1992; and references thereof) and Häkkinen (1993). The original POM code uses centered differencing for advection which can develop undesirable effects for scalar variables (such as unrealistic temperatures) when applied at strong frontal regions, e.g. such an intense front occurs over the Iceland Faroe ridge in the near bottom sigma-layers. In our model, we use a modified upstream differencing scheme based on piecewise parabolic method in the form developed by Lin et al (1994). This scheme is much less diffusive than the regular upstream differencing, however, it still contains numerical diffusion, so we do not apply any explicit horizontal diffusion for T and S.

The model is the same as described in Mauritzen and Häkkinen (1997) and Häkkinen (1998) and the exact choices of boundary conditions are the same. The coupled ice-ocean model extends from the Bering Strait to 15S with resolution of 7/10 in 'longitude', 9/10 in 'latitude' (in a rotated coordinate system with a equator at 30W and the pole at 120W, 0N). There are 20 sigma-levels in the vertical, with higher resolution near surface. The ocean model was initialized with the annual average hydrographic climatology of Levitus (1982). The transports at oceanic lateral boundaries were specified to a 0.8Sv inflow in at the Bering Strait which exits at 15S. T and S at the open boundaries and at the Mediterranean outflow points are relaxed to Levitus values. The topography (derived from the TerrainBase Global DTM data base with 5'x5' resolution) is smoothed so that the topographic slopes are limited to below 1% and grid-to-grid depth variations below 35%. By choosing the two bottom layers to consist of 15% and 20% of the water column we ensure that the water column above the z- level where the deepest pressure gradients are computed lies above the bottom at any given grid interval.

The momentum exchange between the atmosphere and ice/ocean are specified from the Trenberth et al (1989) monthly ECMWF wind stress climatology over open ocean and a geostrophic wind stress (derived from NCAR 5x5 surface pressure climatology) over sea ice with an exchange coefficient of 1.3E-3); the heat exchange with exchange coefficient of 1.3E-3 is derived from the ECMWF monthly climatologies of wind, temperature and humidity and model generated surface

temperature and derived specific humidity with 98% saturation. Short-wave and downward long-wave radiation require cloudiness information which is given by International Satellite Cloud Climatology Project (ISCCP) measurements. The precipitation-evaporation (P-E) field (monthly climatology) is obtained from NMC operational analysis (Rasmusson and Mo, 1997). When the river runoff (from Russell and Miller (1990)) with an annual total of $18000km^3$ is included, modifications were added to the P-E field at 8-12N to conserve salt in the basin.

The model is run 10 years using the above described climatological surface forcing. The COADS climatology was not used for this spinup run because ECMWF produces a more reasonable quasi-equilibrium state. After year 10 the COADS anomalies 1946-1993 (in a 1X1 degree grid, daSilva et al. 1994) are added to the above described climatology everywhere south 70N, with the exception of wind stress and wind speed for which the anomalies are applied south of 60N. North of 50N, the wind stress and wind speed are computed from NCAR pressures and blended over a 10 degree latitude band from 50N to 60N. P-E and cloud forcing remain to be climatological during 48 year simulation. The first 5 years (1946-1950) have been neglected from the analysis as a part of the spinup.

3. Modes of variability

3.1 Decadal cycle in observations

The longest records for any oceanic quantity are the reconstructed SST fields and tide gauge data which both can cover a period over 100 years. Although we cannot address here how exactly the sea level recorded at coastal tide gauges relates to the variability in the open ocean, it is assumed that steric height variations off-shore influences the coastal ocean. It has been known that e.g. the US East Coast tide gauge data contains a strong decadal frequency which has been associated with atmospheric forcing (Maul and Hanson, 1991), as the coastal sea level variability beyond the time scales of continental shelf waves and diurnal and semidiurnal tides is determined by winds and steric height variations off-shore. Greatbatch and Goulding (1989) explain a considerable portion of the seasonal coastal sea level variations in US Eastern Seaboard due to the barotropic response of the ocean to

seasonally changing wind stress curl to which the ocean gyres adjust within one month. Thus it can be expected that tide gauge data contains longer period wind stress curl variability through open ocean barotropic and baroclinic responses as well as the oceanic baroclinic response to changing heat fluxes.

Besides conventional Fourier analysis, the dominant frequencies in SST and tide gauge data were explored using the Singular Spectrum Analysis (SSA) (Vautard et al. 1992) which is a data-adaptive method to analyze signals in short, noisy, and nonstationary time series. SSA is based on principal component analysis (PCA) which solves a lagged covariance matrix of the process. The window within which the time series is decomposed into eigenmodes is supplied by the user and depends on the periodicity of the process under study. In principal, the window should be of length of at least one oscillation period with an upper limit of a typical lifetime of the oscillation, but not more than one third of the time series. A periodic signal can be identified by a near equal pair of eigenvalues. Typically the modes with a physical periodicity are singled out as the first few pairs of eigenelements with the higher modes representing noise in the system.

3.1.1 Decadal cycle in SST

First the SST variability is studied based on the reconstructed 6x6 degree SST fields by Smith et al. (1998) for period 1856-1997. The computation of Empirical Orthogonal Functions (EOF) result in EOF1 with 26% and EOF3 with 11% of the variance for the period 1856-1997 (EOF2 with 15% of the variance has the trend) which are shown in Figs. 1a-b. They are similar to the modes retrieved Deser and Blackmon (1992) from COADS data for the 1900-1989 period, the first modes are the same, but their dipole mode appears here as the 3rd mode. The principal components (PC's) of these modes are shown in Figs. 1c-d with their SSA reconstruction from SSA-modes containing a decadal signal. The PC1 has first two modes with longer frequency than the 31 year window can resolve, the third (4.54% of variance) and fourth (4.52%) modes have a periodicity with about 12 year period. Even though SSA resolves the mode in eigenvalue space, a conventional Fourier analysis (3 50% overlapping subsections and a Hamming window; 10 degrees of freedom) does not have a significant peak above red noise at this period. The pair of SSA modes 6 and 7 from PC3 (Fig. 1d) have decadal

variability at 13-14 years with variance of 4.32-4.40 %. The first 5 modes have a longer period than the window can resolve or contain irregular cycles. The explained variance of 5th mode (4.54%) and the 8th mode (4.10%) do not allow a clear separation in eigenvalue space. Using Fourier analysis (with 3 50% overlapping subsections) the period of 13-14 years is not above the red noise 95% confidence level, however, the later subsection of 70 years has rather strong peak at that periodicity. This is consistent with findings by Deser and Blackmon (1993) whose decadal cycle in SST dipole mode was not significant in respect to red noise. The total variance of the decadal mode, 12-14 years, is only about 3%. Thus the signal is rather weak in SST, and the SSA reconstructions also show that it is nonstationary, with only the recent decades, 1950-90, having a strong regular cycle.

EOF decomposition does not necessarily separate the data fields optimally to highlight the significant frequencies. To avoid possible limitations by EOF's, a spectral analysis is performed directly for SST time series in two distinct areas. EOF's emphasize the locations of the highest variance which are used in choosing areas to create areal average SST time series: an area SE off the coast of Florida is chosen as it is the storm formation area, 18N-30N, 81W-57W, and an area in the subpolar gyre, 42N-60N, 57W-27W, is chosen where modification towards subpolar mode waters and LSW production takes place. These two time series are shown in Fig. 2a. The SSA-decomposition of the southern area gives a decadal period of 14-15 years in the 3rd and 4th modes (well separated), the first two being much longer term variability. The conventional Fourier analysis fails to give any significant decadal periods beyond red noise for this southern time series for monthly data. Using only winter (JFM) anomalies, Fourier analysis (divided into a 3 50% overlapping sections, multiplied by Hamming window) suggests a peak at 14-year period. It is only present in a subsection from 1890 to 1960. When the spectra from the three sections are averaged, the 14 yr peak becomes indistinguishable from the red noise. Clearly this signal is of nonstationary nature as already suggested by SSA-analysis of PC1 and PC3. In contrast, SSA-decomposition for the subpolar time series had difficulty of separating modes because of the very low frequency variability. However, Fourier analysis (using monthly data (1704 points) in three 50% overlapping sections and a Hamming window; 10 degrees of freedom) gives two significant peaks at 14 and 8 years which are significant at 95% level when

compared to red noise, Fig. 2b. The last two 71-year sections determine the significance of the peak at 14 years containing 7-12% of the variance, and 7% overall when the three sections are combined. The peak at 7-9 yr is present in all sections, but narrowed down to 9 years during the last 71 years. Overall 7-9 yr interval has 7% of the variance. The subdecadal frequency in SST has been reported by several authors, e.g. Mann and Park, (1994), and Moron et al. 1998. In the Mann and Park study it is mainly found in the very northern North Atlantic as here. Moron et al. find it to affect the whole North Atlantic.

3.1.2 Decadal cycle in sea level data

The longest tide gauge data from PSML minimum gaps (at most 2 years, exceptions are stated) were chosen for analysis. The gaps were filled by linear interpolation of sea level anomalies and no atmospheric pressure corrections were applied to the data. The low pass filtered tide gauge data along the US east coast is shown in Fig. 3 from north to south. The stations shown have been widely used in literature in studies of sea level variability. The distribution of stations covers latitudes from 20N to 60N, but not all of them are discussed in detail. Latitudes of the tide gauge data referenced below are in Table 1. The northern stations show somewhat more irregular cycles of variability than the southern stations, Charleston, Mayport and Miami. In the case of Mayport and Charleston, the decadal cycle, at about 12 years, is evident to a bare eye and it is quite regular throughout the observation period from 1920's to present. The amplitude of the cycle is about 6 cm (12cm from peak to peak). SSA-modes from Portland, Boston, New York, Atlantic City, Charleston and Mayport are tabulated in Table 1. The window was chosen to be about 1/3 of the record length. The first two SSA-modes for Portland are longer than the window length can resolve, but has modes 3 and 4 which have a periodicity of 7-8 years. In the case of Atlantic City, Charleston and Mayport the decadal frequency at about 12 years exists in the first modes. Boston has a decadal period in 3 and 4 modes while New York tide gauge does not show any decadal or subdecadal periods using SSA. The contribution of the decadal mode to the total variance is high in Atlantic City where the first two modes explain 6.79% and 6.73% of the variance. The same holds for Charleston where the first 2 modes explain 7.08% and 7.01% of the

variance (detrending of the Charleston tide gauge time series was done in two sections, while in all other time time series a single linear trend was removed). The reconstruction of the detrended Charleston sea level from its 1st and 2nd SSA-modes along the seasonally binned data and an 11-season running mean are shown in Fig. 4. The decadal cycle is clearly present in the data with some amplification during the recent decades. The original and SSA-reconstructions of SST mode 1 and of the Charleston tide gauge time series show similar decadal variability, such that a negative sea level lags a positive SST PC1 (a negative subtropical SST, positive subpolar SST) by about 4 years.

On the European side, there are several records over hundred years but some of them have 10-year gaps limiting their use in this time series analysis. A sample of low pass filtered variability at the western Europe is shown in Fig. 5. (Time series at Brest and Aberdeen have been shifted by 30 years forward for convenience). Coherence between the northern and southern stations is not always evident because the eastern North Atlantic is dynamically complicated which is reflected in the sea level: it is an area of subduction of the ventilated isopycnals, the subducted waters will also carry thermal anomalies affecting the steric height and it is also the side of the ocean where coastal upwelling would be found. SSA-modes with decadal frequency for Tenerife (the shortest record with 63 years and contains a 5 year gap 1936-1940, detrending was done in two sections), Lagos, North Shields, Brest, Aberdeen and Bergen are listed in Table 2. In general the first modes are of lower frequency than window length of 21-34 years can resolve, except for Tenerife and N. Shields. Nearly all stations display periods of 10-12 years with exception of Brest and Bergen. At higher latitudes, e.g. at Bergen, a period of 7-8 years appears as the 3rd and 4th modes with 3.8-4.3% of the variance. Fourier analysis using two non-overlapping subsections and a Hamming window confirm the significance of SSA periodicities found. The decadal frequency above noise level is lacking at Brest, Newlyn (Fourier analysis has a 11 year peak) and Cascais. It is unclear why, but it is possible that aliasing of storm surges, tides and seiches (various error sources in monthly mean data is discussed in Pugh (1987) and Sturges (1987); Sturges points out though that much of the aliasing effect for storm surges and tides can be neglected for periods longer than a few years). One could perhaps consider the power at 8-9 years in tide gauge data with some caution because one of the tidal peaks occur at 8.85 years

from the revolution of lunar perigee. However, the occurrence of the 8-9 year peak in high latitude SST gives it credibility. Additionally, other errors from unknown sources may be included, for instance, Cascais and Lagos are only 1 degree apart in latitude, thus one would expect to find the same leading signals in both of them. In fact, the decadal period at Cascais is 16-17 years instead at 10 years as in Lagos. Despite these problems, the European side southern tide gauges have a stronger decadal signal than the northern ones similar to the behavior in the US Eastern Seaboard.

3.1.3 NAO and the decadal and subdecadal cycle in SST and tide gauge data

There appears to be a split in dominant frequencies between the northern and southern tide gauge stations, with a shorter 7-8 year frequency prevalent in the north but a longer 12-14-year cycle dominates the southern, subtropical stations. This dissimilar behaviour between the northern and southern stations has been noted before, e.g. by Thompson (1990) in respect to local wind forcing. The prevalence of the 13-14 year cycle in the SE US tide gauge data (from 1931-1987) has been reported also by Maul and Hanson (1991) from Fourier analysis and by Unal and Ghil (1995) using SSA-analysis. In addition, Maul and Hanson found a strong simultaneous correlation with a NAO-like SLP pattern for wintertime. On the other hand, a 7-8 year period, but not a 13-14 year period, is a significant frequency found in the winter NAO index (Rogers, 1984). Computation of the SSA-modes from the winter NAO index (Hurrell, 1995) using 31 year window gives a pair of modes (3rd and 4th; not shown) which have 8 year periodicity and explain 6.7-7.2% of the variance (again the first 2 modes have longer than 20 year periodicity; the 5th and 6th modes explaining 4.4-4.5% variance have a 2-3 year periodicity). The barotropic response to changes in wind stress curl takes place within a month via barotopic planetary waves (Gill, 1982) which is why this 8 year periodicity should appear in the sea level records: A correlation of Portland winter-average sea level with NAO index (84 winters) gives significant correlations of the same sign at 0 lag (-0.36) and at -7 year lag (-0.42), at other lags correlations are small. A significant correlation at 0 lag can be found also between Bergen sea level and NAO-index (69 winters) (+0.55). No instantaneous correlation was found for the southern tide gauges such as Atlantic City or Charleston. Thus, the instantaneous response in the

Portland and Bergen sea level represents the barotropic response of the ocean to a change in westerlies at a period of about 8 years. Because the barotropic oceanic response becomes stronger at the higher latitudes as the stratification weakens (Gill and Niiler, 1973), the period appears predominantly in the northern tide gauge stations. For the same reason the 14 year period, if it is a result of baroclinic dynamics, should weaken in sea level towards north.

Examination of SSA decompositions of the SST data and tide gauge data on both sides of the Atlantic enforces the idea that there exists two slightly different decadal frequencies. The SST EOF-mode 1 with a dipole structure has about 10 year cycle, while the EOF-mode 3 has about 14 year cycle. A similar split in dedacal or near decadal frequencies occurs in the tide gauge SSA-modes. Despite possible tidal aliasing, the tide gauge data seem to follow physically reasonable behaviour patterns of variability dividing the northern and southern stations. While the subdecadal variability in SST and tide gauge data is limited to the subpolar areas, the longer 12-14 year period can be found in everywhere in SST and in the southern tide gauges. Deser and Blackmon (1993) also note that the variability of the dominant SST EOF1 time series displays slightly different decadal frequencies; about 9 years before 1945 and about 12 years after 1945. The 9 year period in SST does have some justification from the fact that NAO itself has considerable power at periods below 10 years. This is because a SSTA pattern resembling SST EOF1 is a direct response to NAO associated heat fluxes (see Fig 15a, discussed later in detail). How the subdecadal periodicity arises cannot be addresses here, instead this study concentrates on the 13-14 year period which is quite distinguishable in the ocean and leaves an imprint on the atmospheric quantities implying an existence of a distinct coupled mode.

3.2 Net heat flux anomalies

This paper focuses on the role of heat exchange in a possible coupled ocean-atmosphere mode. To construct a coherent and robust picture of heat exchange variations, the heat fluxes from three sources, NCEP, COADS and model modified COADS, have been used. The monthly NCEP net heat flux anomaly data were obtained from the daily reanalysis values subtracting monthly mean values. The dominant modes of the heat flux variability are represented by two EOF patterns (Fig. 6a-b). The

two EOFs account for 17% and 12% of the total variance in NCEP data. Both modes are also found in the COADS (daSilva et al., 1994) heat flux data and in the ocean model modified COADS heat flux data (derived from COADS atmospheric anomalies and the model SST) (Häkkinen, 1998). The first two principal components for NCEP, COADS and model modified COADS are displayed in Figs. 6c-e after being normalized (by one standard deviation), detrended and low pass filtered (37 month Hanning filter). The winter extrema in PC1 and PC2 correspond to heat fluxes associated patterns that have appearance of NAO and WA-like patterns (Cayan, 1992; Häkkinen, 1998). There are apparent discrepancies between the NCEP and COADS derived PC's, and even lower frequency variability than decadal is present. The model modified heat flux and COADS heat flux do differ somewhat in 1990's when COADS and NCEP produce a strong downturn, but the model heat flux stays high. However, the high correlation of the low pass filtered forms of the leading PC's is evident in all three data sets, although less strongly in COADS data. The significant correlations (at 95 % confidence level) using Nov-Apr averages and PC1 leading PC2 are 0.33 at +2 years for NCEP, 0.33 at +4 years for COADS and 0.41 at +1 and +3 years (0.37 at +2 years) for the model. This suggests that the two leading heat flux modes represents the same phenomenon and form a propagating pair. At a lag of 3 years the modes would be in quadrature. Although the correlation between the original COADS PC1 and model heat flux PC1 is high (0.76 for all 516 months), as well that of PC2's (0.83), it will be shown that the dynamics of the ocean model recreates heat flux modes which are internally more consistent than those of COADS. A notable manifestation of this is already seen in the low-frequency correlation of the PC1's and PC2's, where correlation between COADS PC1 and PC2 is not very evident. Due to the differences between the original COADS flux and the model flux in the 1990's, the model flux is used only for period 1951-1990, 40 years which is also the length of the NCEP time series.

The decadal variability is evident in the low pass filtered and detrended PC1 and PC2 (Fig.6c-e). Time series of heat flux PC's are too short to seek validity to the spectral peaks that might exist on decadal frequency, but Fourier line spectrum can be used to estimate the distribution of variance on different frequencies. If one would use monthly anomalies, the low frequency band, periods 10-40 years, would have about 4 % of the variance. If all seasons were used for the power spectrum, the low

frequency domain would receive about 10% of the variance. However, if one selects only winter (DJF) values to emphasize lower frequencies, the power spectrum, e.g. for the model heat flux PC's, concentrates much more of the variance, 40%, to the periods above 10 years (the corresponding fraction is 40% in NCEP heat flux PC1, and 20 % in COADS PC1). Model winter heat flux PC1 contains close to 25% of the variance at about 13 years in PC1 (not shown). COADS winter data does not exhibit the decadal peak as distinctly as the model heat flux, while NCEP winter PC1 has 37% of the variance at 10-13 year periods (not shown). As seen the subpolar SST has a significant period at about 8 years which should appear in the heat flux also as a proof of consistent underlying physics. When the winter (DJF) subpolar heat flux (average from 45N to 65N) is subjected to a Fourier analysis, strong peaks appear at about 13 years and at 8 years (not shown), the latter is present also in the winter COADS data. In NCEP subpolar flux, the 8 year period has a large fraction of variance but is not separated peak in the cluster of periods between 8-13 years with a large power (46% of the winter variance). To emphasize the fact that the low frequency signal is mainly found during winter months, the subpolar heat flux anomalies from NCEP reanalysis are shown as monthly values (Fig. 7a) and winter (DJF) values (Fig. 7b) both with the Fourier reconstruction from periods at 8-13.3 years. In conclusion, the SST, sea level and heat flux at the subpolar latitudes all contain considerable power at the same decadal and subdecadal frequencies.

4. Decadal oscillation for the last 40 years

4.1 The half cycle

The question whether the power at 12-14 years in SST, sea level and heat fluxes originates from intrinsic atmospheric low-frequency processes or due to the coupling with ocean is the heart of the problem in determining the role of the ocean in the decadal climate variability. The hypothesis of the coupled cycle to be constructed is that it is tied to the thermohaline circulation driven by surface heat fluxes. The thermohaline cell variability associated with this hypothesis involves only the water masses immediately below the permanent thermocline, i.e. waters of the subpolar origin including LSW as shown in Häkkinen (1998). If there is a connection, one should be able to construct the 12-

14 cycle, or at least a half cycle, from lagged composites or correlations based on some integral measure of the heat flux variability. As discussed above, the Fourier analysis of winter averages of the heat flux PC1 contains strong power on decadal frequency, thus PC1 is chosen to build composites of the seasonal mean SLP, net heat flux and SST etc. Furthermore, the low frequency part of the heat flux PC1 is linked the to strength of the thermohaline cell (Häkkinen, 1998). The ocean model simulated SST and upper ocean heat content anomalies (OHCA) (= the average temperature in the top 1000 meters) are also used to highlight the changes in thermohaline circulation. All data, heat flux PC1's and the data fields, are linearly detrended before computing the composites. Composites to be shown cover typically a time-span of 4 seasons before to 24-48 seasons after the magnitude of winter (DJF) heat flux PC1 is above one standard deviation. The years of these winters with extreme heat flux PC1 (above one std; based on all seasons) are listed in Table 3 for NCEP, COADS and MODEL. Results will be presented as the difference of positive and negative composites, altogether consisting about half of the winters in the time series at lag=0. Similar composites were obtained from COADS and from an ocean model modified heat flux and SST data and are shown in some cases. When compositing NCEP/NCAR data, NCEP heat flux PC1 is used; for COADS data, COADS heat flux PC1 is used, and for model data, model heat flux PC1 is used. The ocean model results are used to elucidate the heat content changes in conjunction of the decadal mode.

As previously noted the heat flux EOF1 and EOF2 correspond to NAO and WA-like SLP patterns, further support is offered to suggest that they represent the same phenomenon by computing lagged correlations of PC1 and PC2 from the model heat flux with the NCAR SLP field. The correlations are shown in Figs. 8 when the winter data (binned as DJF; 39 winters), 0.3 is a significant correlation at 95% confidence level. Fig. 8, at 0 lag, as expected show the NAO SLP pattern and its remnants for the next 2 years. At year 3, the highest correlation occur off Newfoundland centered at about 45N, 50W, and the pattern resembles the WA pattern (Wallace and Gutzler (1981) teleconnection center is at (55N, 55W), but their SLP WA-composite has the northern center at (60N, 40W)). Year 6 (and 7) show reversal of the spatial pattern at 0 lag. Similarly, the lagged correlations are shown for PC2 in Figs. 9 where 0 lag pattern show WA-like pattern centered at (50N, 45W). Year

two shows a low still in the subpolar gyre, but year 3 shows an existence more or less of the negative phase of NAO with the low around Azores being significant, but the northern high center correlations are not significant. Years 6-7 show initiation of the reversal of the pattern at 0 lag, however only the southern centers have significant correlations. Thus, the (model) heat flux PC1 and PC2 recover each other's SLP patterns 3 years after the height of their parent SLP patterns, and to some degree also the reversal of these parent patterns 6-7 years later.

Besides the lagged correlations, composites of SLP can be constructed at the extrema of heat flux PC1 to build a coherent picture of the cycle. The composites for the model heat flux PC1 are shown in Figs. 10. The lag 0 composite naturally is the NAO SLP pattern, but by the summer of year 2, a weak low pressure anomaly appears east of Newfoundland at mid-ocean. It grows into a 2-3 hPa anomaly by year 3. This pattern resembles the WA-like teleconnection with a low centered at (45N, 45W). At year 6 the SLP composite pattern has properties of the reverse of the lag 0 pattern, but again, only the difference values at the southern center are significant. The pressure anomalies at years 3 and 6 are of the similar strength as in the decadal mode of Grötzner et al. (1998). The composites for NCEP heat flux PC1 and NCAR SLP data (only available until 1995; not shown) suggest that the mid-phase WA-like pattern is prominent during summers at year 1.5 and 2.5 and reversal takes place at 6 years. Overall, both the correlations and composites suggest a close relationship between NAO and WA-like SLP patterns at low frequencies.

To demonstrate the evolution of the decadal heat flux cycle in itself, the heat flux is composited against the its PC1 extrema from -1/0 to 5/7 years in Fig 11-13 using NCEP, COADS and model modified COADS data (NCEP and model uses 40 years of data, COADS 48 years). At lag =0, COADS heat flux PC1 has only 21 extrema above one std during 48 years, both model and NCEP PC1 have 24 extrema in 40 years. Slightly different time-lag spans are used to elucidate the clearest signal present in the time series. Since the cycle is weak, depending on the data set used, different aspects of the cycle are recovered to various degrees as seen from Figs. 11-13. Besides the self-evident maximum at lag 0 in all three composite sets, in NCEP data (Figs. 11) the NAO -like heat flux pattern is already present at year -1. Some of the NAO-related pattern is still left on year 1 and 2. By

year 3, a heat flux center over the Gulf Stream-N. Atlantic Current (NAC) area has developed and it resembles heat flux EOF2 in all composite sets. Year 4 is not shown, but by year 5, traces of a pattern opposite to year -1 has developed. At year 5, less than 50% of amplitude is recovered in NCEP data. Also the mid-cycle amplitude of 30W/m2 is only 40% of the maximum value of heat flux when composited against heat flux PC2. The COADS and model heat flux composites for years 0 to 6-7 (Figs. 12-13) are similar to the NCEP ones. The mid-cycle pattern is less strongly represented in the COADS data than in the model or NCEP heat flux data. However, the reversal is well defined in both data sets. The reversal in COADS data takes place with a 6 year period as in NCEP data, and recovers about 50 % of the amplitude in the subtropics. In the model heat flux, the mid-cycle pattern is well defined and stretches along the Gulf Stream and North Atlantic Current. Reversal of the pattern takes about 7 years in the model data, and with nearly the same strength as the original signal in the subpolar gyre. This heat flux cycle indirectly measures the movement of storm tracks from the high index phase of NAO to WA and then to low index phase of NAO. The above PC1 and SLP correlations and composites complement the picture of the negative SLP anomaly moving from north to south.

For the different phases of the cycle, we construct composites for SST (from Smith et al. 1996) used in NCEP Reanalysis and corresponding NCEP heat flux PC1 (Figs. 14), and for model SST based on model heat flux PC1 (Figs. 15). Similarly composites for OHC from the model are based on the model heat flux PC1. Below we mainly discuss the NCEP data in connection of SST composites, because we want to rely as much as possible on "observational" data. The model and Reanalysis composites are very similar but the NCEP composites have more smoother and broader patterns than the model derived.

a) Years -1-0: Local response

At one year before (DJF, year -1) the maximum positive phase of the EOF1, the NAO dipole can be found in heat flux anomalies (Figs. 11) but only weak anomalies in SST and OHC (not shown). At DJF, year 0, the high index phase of the NAO, heat flux anomalies (Figs. 11a-b) are organized as a dipole with positive values in the Labrador Sea and negative values off the US south-

east coast as shown by Cayan (1992). It has been shown previously by e.g. Deser and Blackmon (1993) that stronger than normal westerly winds are associated with positive heat flux anomalies and coincide with cooler than normal SSTs. Southerly winds are associated with negative heat flux anomalies off the US east coast. This results in the SST composite which shows the well-known SSTA dipole with warm subtropics and a cold subpolar gyre (Fig. 14a). The dipole is a local response to the atmospheric circulation as concluded by Deser and Blackmon (1993). The OHC anomalies (Fig. 16a) are still weak and follow the SSTA. The simulated March mixed layer depth composite at year 0 corresponding to the DJF extremum of model heat flux PC1 (Fig. 17a) shows the anomalously deep mixed layers everywhere in the subpolar gyre but especially at the center of the Labrador Sea. March of the year 0 has the largest positive mixed layer depth anomalies during the cycle indicating the maximum deep convection. The influence of the deep convection as enhanced overturning will be felt about 2 years later in the mid-latitudes (Häkkinen, 1998).

b) Years 1-2: Advection

Sutton and Allen (1997) show that the SSTA anomalies appear to advect slowly along the Gulf Stream. This slow advection, 2cm/s, is shown by Saravanan and McWillams (1998) to be a typical average speed of the top 500 meters in the Gulf Stream area. In NCEP data, by MAM of Year 0, positive SSTA (Fig. 14b) reaches the central Atlantic with a maximum at (40-45N, 40W) which coincides with the positive anomaly center of the heat flux EOF2 (Fig. 6b). By year 2 (shown for model in Fig.15c), warm SSTA has spread away from the North American coast.

The warm water migration is not limited to the surface, the warm anomalies extending down to the thermocline (at 1000-1200 meters at 25N) appear to propagate in consort (Fig. 16b-c). The OHC anomaly in the Gulf Stream region accumulates due to the local heating, but also due to deepening of the isopycnals (not shown), i.e. ocean dynamics are important to the build-up of the thermal anomaly. The composites do show westward propagating heat anomalies at latitudes 20N-30N which is a sign of Rossby waves. This phase, 1-2 years after the maximum in PC1, is also associated with the maximum MOC and poleward oceanic heat transport (Häkkinen, 1998). As a result, by the end of

year 2 (Fig. 16c), the subtropical positive OHCA begins to advect north-east along the NAC. The subpolar negative OHCA is seen to escape to the slope waters from year 1, thus the decadal SSTA is out of phase in the Gulf Stream and the slope waters as in Kushnir (1994).

c) Year 3: Feedback from the ocean

By DJF Year 3, the warm SSTA in the mid-Atlantic and the cold SSTA in the Labrador Sea have persisted for more than 2 years, Fig. 14d. The upper ocean has a higher than normal heat content covering the ocean basin north of 40N (Fig. 16d), with a maximum co-located with the SST maximum (fig. 15d). A negative SSTA is seen in the slope waters in the model composites Fig. 15d which is reminescent to SSTA composite of Kushnir (1994) (his figure 5b). At this time, the mid-ocean is covered with positive heat flux anomalies (Fig. 11e) directly atop of the positive SSTA. The heat flux anomaly pattern resembles the EOF2 (Fig.6b) with positive anomalies centered at (40-45N, 40W) and negative anomalies to the north. At this time, Fig. 10d, a low pressure anomaly cyclone has formed N-NE of the area of warm SSTA resembling WA-pattern. This SLP pattern has its southern section which is associated with geostrophic off-shore wind field (bringing cold continental air) overlaying the positive heat flux (Fig. 11e) and SST (Fig. 15d) anomalies. It is significant that the EOF2 heat loss pattern overlays a positive SSTA, because one would expect a negative SST to be associated with a heat loss. Thus, the relationship between the heat flux pattern EOF2 and underlying ocean is different depending on the frequency band. This phase has similarities with the idealized numerical experiments by Kushnir and Held (1996) who show a low (high) forming downstream of a positive (negative) mid-latitude SST anomaly. A simultaneous relationship between the height anomalies and warm SSTA in the middle of the Atlantic during cold seasons has been reported by Wallace and Jiang (1987). However, they interpreted this as the WA pattern forcing the SST anomalies. The study of Kushnir (1994) on interdecadal variations in the N. Atlantic indicated that mechanisms for interannual and decadal variations may be different. He shows SSTA pattern similar to composites Fig. 14d and 15d to be associated with a low in the mid-basin centered at about 45N. The location of this low is at about the same as the one pictured in Fig. 10d. Here long lasting heat build up in the mid-ocean basin

may be the key to the changes in the atmospheric circulation. Once the heat flux similar to the EOF2 pattern establishes itself, it damps the SSTA in the Gulf Stream/North Atlantic Current area but enhances the SSTA in the northern subpolar gyre. The damping of the mid-basin SST was suggested also by Kushnir (1994) based on wind anomalies, but the use of the heat flux anomalies directly puts his conclusion into the framework of the coupled cycle itself.

d) Years 4-7: Completion of a half cycle

By year 6 the north-south dipole in the SLP anomaly field is out of phase with that of DJF year 0 (Fig. 10g). The net heat flux anomaly pattern of DJF year 5 (NCEP; Fig. 11f) and 6-7 (model; Fig. 13e-f) is similar to the negative phase of EOF1. After year 3, the mid-ocean SSTA decreases, but there is a significant positive SSTA and OHCA circulating the subpolar gyre and a lesser anomaly in the NAC area at year 6-7 (Fig. 14e-f and 16e-f). The local influence of atmospheric fluxes appears to take effect and the ocean responds to the atmospheric anomalies; a cold SSTA in subtropics and a warm subpolar SSTA and OHCA (e.g. Fig. 11f, Fig. 13f). Thus, subpolar surface waters are so warm that no deep mixing is taking place which is corroborated by the most negative values of the model simulated March mixed layer depth anomaly composited against the model heat flux PC1 at year 7 (Fig. 17b). This indicates that deep convection is at its minimum at this time during the cycle. Advection with the slope waters and subduction into the thermocline waters are the only ways the positive OHCA can be removed from the subpolar gyre. Since the surface waters do not sink below the thermocline, the thermohaline cell and meridional heat transport weaken.

The relation between SSTA and heat flux in the subpolar gyre is a significant aspect of the cycle: If one accepts the hypothesis of a cycle where these anomalies advected from subtropics as suggested by the previous composites, a justifiable interpretation is that there is a positive feedback where the atmospheric fluxes are amplifying SSTA in disquise of a local oceanic responce to heat fluxes. The lack of atmospheric damping of the decadal SSTA in the subpolar gyre was pointed out by Kushnir (1994). Also, in the model of Grötzner et al. (1998) the subpolar SSTA and heat flux correlation stays high for lags where ocean leads which is interpreted as positive feedback. The

amplification of SSTA and OHCA in the subpolar gyre defines the area of unstable air-sea interaction where local heat fluxes force the ocean either to a state of maximum convection or to a state of no convection as demonstrated by the composite differences of the model simulated March mixed layer depth anomaly (Figs. 17a-b). The oceanic adjustment to the changes in buoyancy flux, and associated deep convection, will be baroclinic with a delay of several years via baroclinic Rossby waves (Wajsowicz, 1986). In effect, the variability in the thermohaline circulation which caused the formation of the subtropical SSTA and OHCA in the first place, creates a negative feedback on itself through the northward advection of the heat anomalies. This negative feedback is further amplified by the atmosphere-ocean heat exchange.

Now after year 6-7, the same processes with opposite sign are ready to begin: a weakening thermohaline cell creates a negative heat content anomaly in the subtropics which will influence the atmosphere while it starts to advect northwards. Another 6-7 years later one arrives to the state depicted by lag 0 composites.

4.2 The decadal oscillation and the ocean as a low pass filter

Even though the cycle described above is weak, less than 5 % of the monthly variance in the surface heat flux and SST, the power at decadal and longer frequencies should increase when quantitites involving deeper ocean are concerned. To demonstrate the efficiency of the ocean as low-pass filter, the simulated upper ocean heat content variability deserves some elaboration. The first two EOF's of the detrended 1000 m heat content (OHC) are shown in Fig. 18a,b and their PC's in Fig. 18c,d. The first two modes explain 12 and 8 % of the total variance. The EOF1 is very similar to the heat content composite at year 3 (Fig. 17d) and depicts the warming of the Gulf Stream and North Atlantic current areas. The second mode has resemblance to the leading heat flux pattern in the northern part, and can be interpreted to reflect the influence of the local heat flux. However, the subtropical part has an eastward extension indicating propagation of heat content anomalies from the east as Rossby waves. The corresponding PC's have most of their power at lower frequencies. In fact, Fourier analysis indicates that over 45% of their variance is at periods longer than 10 years (using

40 years of monthly data). Furthermore, the two OHC PC's are highly correlated, using only Nov-Apr average values, the correlation is 0.65, PC2 leading PC1 by 3 years. This relation is apparent when one considers the composites in Figs. 17 by equating heat flux PC1 with OHC PC2. Again, a propagating pair in quadrature is a valid description of the two first modes of OHC. Although there are only 3 cycles, OHC PC2 shows the quasi-decadal peaks at 1960, 1974 and 1986.

5. Discussion

This study has presented an analysis of a decadal, 12-14 year mode in the North Atlantic from NCEP and COADS data and from an ocean model which was forced with COADS anomalies to highlight the upper ocean (1000m) changes associated with the cycle. Observational data were analyzed to explore the strength and stationarity of a decadal mode in the ocean. There are only two oceanic quantities with time series extending over 100 years which could give statistically significant information on the frequency of the mode and its frequency modulation: reconstructed SST's (Smith et al. 1998) and tide gauge data (from PMSL) go back to the mid-1800's. The SST data decomposed into EOF modes (unrotated) show that the PC of the 1st mode which is similar to the first mode of Deser and Blackmon (1993), has a cycle with 12 year period using SSA. The dipole SST mode (EOF3) shows a mode with about 12-14 year period. Both of the these cyles have only about 3% of variance. The SSA reconstruction of PC1 indicates nonstationarity with strong signal apparent since 1940's. A spectral analysis of the original data in two specific locations, SE of the Florida coast and in the subpolar gyre, finds the same 12-14 year decadal signal but significantly different from red noise only in the subpolar gyre. Also, a significant subdecadal (8 years) signal exists in the subpolar gyre. The two periods have about 7% of the variance each in the Fourier analysis of the subpolar SST. The subdecadal period exists also in the winter North Atlantic Oscillation (NAO) index and subpolar winter heat flux values in COADS and model data. The SSA analysis of the longest tide gauge time series gives a significant periods around 10-14 years if the tide gauge data is from subtropics (e.g. Atlantic City, Charleston, Tenerife, Lagos). If the data is from higher latitudes (e.g. Portland Maine, New York, N. Shields, Bergen), the significant modes have periods of 7-8 years. Thus, SST and tide

gauge data indicate that there exist two dominant periods, one at 12-14 year period and the other one at 7-8 years. The decadal peak in sea level records at 10-13 years has been reported by Maul and Hanson (1991) and Unal and Ghil (1995). The equally weak, subdecadal peak is also found in the winter NAO index by Hurrell (1995) and in SST by Moron et al. (1998) and by Mann and Park (1994).

Besides the presence of the subdecadal period in both the northern tide gauges and NAO-index, the coastal sea level at northern latitudes, e.g. Portland and Bergen, and NAO index (winter values) is correlated at 95% confidence level at zero lag. This indicates that the subdecadal period in sea level is related to the barotropic response of the ocean. On the other hand, the 12-14 year period is a mode at which the baroclinic oceanic response can operate; it is about twice the first baroclinic Rossby wave transmission time at the mid-latitudes (Anderson et al. 1979). At this time it is unclear how to reconcile the two periodicities associated with NAO in atmosphere and ocean. The heat flux variability from NCEP, COADS and model simulations contain similar decadal cycle and additionally the subpolar heat flux exhibits strong power on the subdecadal frequency. The decadal oscillation is weak consisting typically 5-10% of the variance if monthly or seasonal data is considered. However, if one focuses on winter season, the fraction of variance on the decadal frequencies increases to 10-20% depending on the quantity and time period.

The local oceanic response to the NAO forcing and the advection of SSTA along the Gulf Stream/NAC system have been suggested by Sutton and Allen (1997) and Kushnir et al. (1997) to be responsible for the decadal cycle. Here a coupled cycle has been proposed based on the variability in the heat flux which is also responsible for the observed cycle in SSTA. Relations to tropical or sea ice variability were not searched although Deser and Blackmon (1993) have reported that positive sea ice anomalies precede the cold winter SST anomalies in the subpolar gyre. Sea ice is likely to participate to some degree to enhance the cycle, but the participation is more or less passive: During the high index phase of NAO, when the subpolar heat flux is at its maximum, the Arctic ice export of ice is decreased, and vice versa at the low index NAO (Häkkinen and Geiger 1998). Also, the relation between atmosphere and sea ice is shown to be a one-way interaction with atmosphere forcing sea ice (Fang and Wallace 1994) which relation also applies to the Labrador Sea ice cover (Deser et al. 1998).

During the coupled cycle proposed here, an active sea ice participation is not necessary because the SST and OHC anomalies are created in subtropics, not in the subpolar gyre. This is not to say that processes in the northern center of action, the Labrador Sea, are unimportant. On the contrary, the subpolar convection, or lack of it, depends both on the local heat and fresh water flux but also on the heat content of the upper water column advected to the gyre from subtropics. The Labrador sea convection provides the essential tie to the variability of the thermohaline circulation. One requirement for a coupled mode is an existence of an unstable air-sea interaction. In the North Atlantic mode the Labrador Sea is the area of unstable air-sea interaction where local heat fluxes force the ocean either to a state of maximum convection or to a state of no convection. The ocean response to these changes will be baroclinic with a delay of several years as the baroclinic Rossby waves have to across the basin to complete the adjustment to the buoyancy fluxes (Wajsowicz, 1986).

Table 4 sums up the oceanic and atmospheric changes during a half cycle. The significant finding is that this cycle can be constructed based on the leading mode of the surface heat flux. Thus the cycle is directly tied to a quantity which couples the atmospheric and oceanic dynamics. This connection to the surface heat flux also implicates the participation of the thermohaline circulation in the decadal cycle. A similar coupled mode has been observed in a coupled GCM (Grötzner et al (1998)) which they attribute to the advection of SSTA and OHCA resulting from wind driven changes in the subropical gyre circulation. On the other hand, in the model of Timmermann et al. (1998) the role of the thermohaline circulation is invoked in an interdecadal mode of about 35 year period: The overturning regulates the SST anomalies in the subtropics which in turn influence NAO and associated evaporation field and causing surface salinity anomalies at high latitudes. As a net result, the salinity anomalies modulate the overtuning variability in their interdecadal mode. Here the presented decadal cycle is similar as it also relies on the thermohaline cell variability and its feedbacks on itself. However, results here emphasize the importance of the thermal forcing without invoking SSS changes and in a shorter time scale: The warm SSTA and OHCA anomalies are generated in subtropics as a part of adjustment to increased buoyancy fluxes, i.e. by strenthgening overturning. The atmospheric response to these mid-latitude SST/OHC anomalies is a southward movement of storm tracks

indirectly captured by the time evolution of the heat flux field during the cycle where heat flux EOF1 and EOF2 form a propagating pair. The oceanic heat anomalies then move to the subpolar gyre, while they may be damped by EOF2-like fluxes at the mid-ocean (35N-45N), much of the anomalies survive to the subpolar gyre where they are exposed to local flux that amplifies them. The positive feedback at subpolar latitudes is inferred in several studies, e.g. from the model by Grötzner et al. (1998) and from observations by Kushnir (1994). The heat flux variability in the subpolar gyre is of importance for the ocean response in this decadal cycle because it ultimately modulates the strength of overturning. The strong MOC has a negative feedback on itself as the strengthened MOC fills the upper subpolar gyre with low density (=warm) waters. At the half-way point of the cycle, the local heat flux is providing more heat to the upper ocean, positive feedback between atmosphere and ocean, and further amplifying the negative feedback, within the ocean, arising from the overturning. Both of these factors bring the deep convection to a halt, and the adjustment to the new surface fluxes starts at the mid-latitudes through appearance of negative heat content anomalies associated with a weakened overturning. Invoking only gyre transport changes originating from wind stress curl changes can explain SST and heat content anomalies in subtropics, but it is inadequate to account for the role of the significant SST and heat flux anomalies in the subpolar gyre.

As discussed by Grötzner et al. (1998), the North Atlantic coupled mode carries some resemblance with the El Nino delayed oscillator where the Rossby adjustment gives the delay that allows to the system to oscillate (Suarez and Schopf, 1988). The pycnocline depth changes are essential in creating deep, long lived heat content anomalies off Cape Hatteras, which is a storm formation area. The heat content anomalies modify the storm path and change the prevailing wind stress patterns and heat fluxes. There are other similarities with El Nino also: we fully expect that the coupled mode will exhibit non-stationarity depending on longer term variability and noise present in the coupled system. While the recent decades since 1940's show a rather clear 12-14 year cyclicity found in many observables, SST, mixed layer salinities, and sea level changes, the historical SST data gives a hint that this mode may not have been active during the early 1900's.

Acknowledgements: This paper has greatly benefited from discussions with Dr. Kingtse Mo and from her help and insights along the way. Challenging questions and comments from Dr. Clara Deser are greatly appreciated. I gratefully acknowledge the support from NASA Headquarters and NOAA for this work.

References:

Alexander, M.A, and J.D. Scott, 1997: Surface Flux Variability over the North Pacific and North Atlantic Oceans, J. of Climate, 10, 2963-2978.

Anderson, D.T., K. Bryan, A.E. Gill, and R.C. Pacanowski, 1979: The transient Response of the North Atlantic: Some Model Studies, J. Geophys. Res., 84, 4795-4815.

Battisti, D. S., U. S. Bhatt and M. A. Alexander, 1995: A modeling study of the interannual variability in the wintertime North Atlantic ocean. J. Climate, 8, 3067-3083.

Bjerknes, J., 1964: Atlantic air-sea interaction, Adv. in Geophys., 10, 1-82.

Cayan, D., 1992: Latent and sensible heat flux anomalies over the Northern Oceans: The connection to monthly atmospheric circulation. J. Climate 5, 354-369.

daSilva, A.M, C.C. Young, S. Levitus, 1994: Atlas of surface marine data 1994, Volume 1, Algorithms and procedures, NOAA Atlas Series.

Deser, C., and M. L. Blackmon, 1993: Surface climate variations over the North Atlantic Ocean during winter 1900-1989. J. Climate 6, 1743-1753.

Deser, C., J.E. Walsh, and M.S. Timlin, 1998: Arctic sea ice variability in the context of recent wintertime atmospheric circulation trends, submitted to J. Climate.

Fang, Z., and J.M. Wallace, 1994: Arctic sea ice variability on a timescale of weeks and its relation to atmospheric forcing, J. Climate, 7, 1897-1914.

Greatbatch, R.J., and A. Goulding, 1989: Seasonal Variations in a Linear barotropic Model of the North Atlantic driven by a Hellerman and Rosenstein Wind Stress Field, J. Phys. Oceanogr., 19, 572-595.

Gill, A.E., and P.P. Niiler, 1973: The theory of the seasonal variability in the ocean, Deep Sea Res., 20, 141-177.

Gill, A.E., 1982: Atmosphere-Ocean Dynamics, Academic Press, New York, pp 662.

Grötzner, A., M. Latif and T.P. Barnett, 1998: A decadal climate cycle in the North Atlantic Ocean as simulated by the ECHO coupled GCM, J. Climate, 11, 831-847.

Hurrell, J.W., 1995: Decadal Trends in the North Atlantic Oscillation regional temperatures and precipitation, Science, 269, 676-679.

Häkkinen, S., 1993: An Arctic source for the Great Salinity Anomaly: A simulation of the Arctic ice ocean system for 1955-1975, J. Geophys. Res., 98, 16397-16410.

Häkkinen, S., 1998: Variability of the simulated meridional heat transport in the North Atlantic for the period 1951-1993. J. Geophys. Res., accepted with revisions.

Häkkinen, S., and C.A. Geiger, 1998: Low frequency variability of a simulated Arctic ice-ocean system for the period 1951-1993, submitted to J. Climate.

Häkkinen, S. and G.L. Mellor, 1992: Modeling the seasonal variability of the coupled Arctic ice-ocean system, J. Geophys. Res., 97, 20285-20304.

Kushnir, Y., 1994: Interdecadal variations in North Atlantic sea surface temperature and associated atmospheric conditions, J. Climate, 7, 141-157.

Kushnir, Y., Y. Tourre, and B. Rajagopalan, 1997: Decadal and multidecadal variability in Atlantic SST and sea level pressure, submitted to J. Climate.

Latif, M., and T.P. Barnett, 1994: Causes of decadal variability over the North Pacific and North America, Science, 266, 635-637.

Levitus, S., 1982: Climatological atlas of the world ocean, NOAA publ. 13, US Dept of Commerce, Wash. DC, 173 pp.

Lin, S.-J., W.C. Chao, Y.C. Sud, and G.K. Walker, 1994: A class of van Leer-type transport schemes and its application to the moisture transport in a general circulation model, Mon. Wea. Rev., 122, 1575-1593.

Mann, M.E. and J. Park, 1994: Global-scale modes of surface temperature varaibility on interannual to century timescales, J. Geophys. Res., 99, 25819-25833.

Maul, G.A., and K. Hanson, 1991: Interannual Coherence between North Atlantic atmospheric surface pressure and composite southern U.S.A. sea level, Geophys. Res. Lett., 18, 653-656.

Mauritzen, C. and S. Häkkinen, 1997: Influence of sea ice on the thermohaline circulation in the Arctic-North Atlantic Ocean, Geophys. Res. Lett., 24, 3257-3260.

Moron, V., R. Vautard, and M. Ghil, 1998: Trends, interdecadal and interannual oscillations in global sea-surface temperatures, Clim. Dyn., 14, 545-569.

Neelin, D. , D.S. Battisti, A.C. Hirst, F-F. Jin, Y. Wakata, T.Yamagata, and S.E. Zebiak, ENSO theory, J. Geophys. Res., 103, 14261-14290.

Pugh, D.T., 1987: "Tides, Surges and Mean Sea Level", Chichester: John Wiley et Sons Ltd.,472 pp.

Rasmusson, E.M. and K.Mo, 1997: Large scale atmospheric moisture cycling as evaluated from NMC global analysis and forecast products, J. Climate, 9, 3276-3297.

Reverdin, G., D. Cayan, and Y. Kushnir, 1997: Decadal variability of hydrography in the upper northern Atlantic, 1948-1990, J. Geophys. Res., 102, 8505-8532.

Rogers, J. C., 1984: The association between the North Atlantic Oscillation and the Southern Oscillation in the northern hemisphere, Mon. Wea. Rev., 112, 1999-2015.

Russell G.L. and J.R. Miller, 1990: Global river runoff calculated from a global atmospheric general circulation model, J. of Hydrology, 117, 241-254.

Saravanan R. and J.C. McWilliams, 1998: Adjective ocean-atmosphere interactions: an analytical stochastic model with implications for decadal variability, J. Climate, 11, 165-188.

Suarez, M.J. and P.S. Schopf, 1988: A delayed action oscillator for ENSO, J. Atmos. Sci., 45, 3283-3287.

Smith, T.M., R.W. Reynolds, R.E. Livezey and D.C. Stokes, 1996: Reconstruction of historical sea surface temperatures using empirical orthogonal functions, J. Climate, 9, 1403-1420.

Smith, T.M., R.E. Livezey and S.S. Shen, 1998: An improved method for analyzing sparse and irregularly distributed SST data on a regular grid: Tropical Pacific Ocean, J. Climate, 11, 1717-1729.

Sturges, W., 1987: Large-Scale Coherence of Sea level at Very Low frequencies, J. of Phys. Ocean., 17, 2084-2094.

Sutton, R. T., and M. R. Allen, 1997: Decadal predictability of North Atlantic sea surface temperature and climate. Nature, 388, 563-567.

Thompson, K.R., 1990: North Atlantic Sea Level and Circulation in Sea Level Change Studies in Geophysics, National Acad. Press, pp 52-62.

Timmermann, A., M. Latif, R. Voss, A. Grötzner, 1998: Northern hemisphere interdecadal variability: A coupled air-sea mode, J. Climate, 11, 1906-1931.

Trenberth, K., J.G. Olson, and W.G. Large, 1989: A global ocean wind stress climatology based on ECMWF analyses, NCAR Technical note, NCAR/TN-338+STR, 93pp.

Unal, Y.S. and Ghil, M., 1995: Interannual and inerdecadal oscilation patterns in sea level, Clim. Dyn. 11, 255-278.

Vautard R., P. Yiou, and M. Ghil, 1992: Singular Spectrum analysis : A toolkit for short, noisy chaotic signals, Physica D., 58, 95-126.

Wajsowicz, R., 1986: Adjustment of the Ocean under Buoyancy Forces. Part II: The Role of Planetary Waves, J. of Phys. Ocean., 16, 2115-2136.

Wallace, J. M., and Q. Jiang, 1987: On the observed structure of the interannual variability of the atmosphere-ocean climate system. Atmosphere and Oceanic Variability. R. Met. Soc., H. Cattle Ed., 17-43.

Weisse R, U. Mikolajewicz, and E. Maier-Reimer, 1994: Decadal Variability of the North Atlantic in a general circulation model, J. Geophys. Res., 99, 12411-12421.

FIGURE CAPTIONS

Fig. 1 The leading EOF's of winter (JFM) SST for 1856-1997 : a) EOF1 and b) EOF3. EOF2 is similar to EOF1 but its PC contains a trend. Contour interval is 0.2 non-dimensional units. The corresponding time series of c) PC1 and d) PC2 (thin solid) and their SSA-reconstruction (thick solid line). The units for PC's are in Celcius, SSA-curves are multiplied by constant to highlight the decadal cycles.

Fig. 2 (a) Winter (JFM) SST time series (in Celsius) of the subtropical area, SE off Florida, (18N-30N, 81W-57W) and subpolar area (+1C offset) (42N-66N, 57W-27W). (b) Power spectrum of subpolar SSTA time series (monthly data, Hamming window): average over three 50% overlapping subsections (thick). Red noise (thin solid) and its 95% confidence limit (dotted) are shown also.

Fig. 3 A sample of low pass filtered (35 month running mean) tide gauge data along the East Coast of North America. Units are in mm.

Fig. 4 The Charleston tide gauge data binned seasonally and detrended (thin line), its 11-season running mean (dashed solid line), and its SSA mode 1 and 2 reconstruction (thick solid line).

Fig. 5 A sample of tide gauge data from the western Europe detrended and low pass filtered with 35 month running mean. Aberdeen and Brest shifted forward by 30 years for convenience of spanning a similar record length. Units are in mm.

Fig. 6 (a) EOF 1 and (b) EOF 2 of the North Atlantic net heat flux anomalies based on the NCEP/NCAR reanalysis. Contour interval: 0.2, nondimentional unit. The PC's of the two leading heat flux EOF patterns, linearly detrended, normalized by their respective standard deviations and low pass filtered (37-month Hanning filter); (c) NCEP, (d) COADS, and (e) model. The thick line is PC1 and the thin line is PC2.

Fig. 7 The subpolar heat flux anomaly (thin lines) from NCEP/NCAR reanalysis as (a) monthly values, and as (b) winter (DJF) values. Thick solid lines represent reconstruction of the time series including only Fourier components at periods 8, 10 and 13.3 years.

Fig. 8 Correlations between model heat flux PC1 and NCAR 5x5 SLP fields for time period 1951-1990. Only seasonal averages for DJF are used. 0.3 is a significant correlation at 95% level. a) lag 0, PC1 leading SLP at b) lag 1 yrs, c) lag 3 yrs, d) lag 4 yrs, e) 5 yrs and f) 7 yrs.

Fig. 9 Correlations between model heat flux PC2 and NCAR 5x5 SLP fields for time period 1951-1990. Only seasonal averages for DJF are used. 0.3 is a significant correlation at 95% level. a) lag 0, PC2 leading SLP at b) lag 1 yrs, c) lag 3 yrs, d) lag 4 yrs, e) 5 yrs and f) 6 yrs.

Fig. 10 SLP (from NCAR 5x5 data) composite difference at the extrema of model heat flux PC1, all seasons above 1 std (DJF, MAM etc, 1951-1990) are counted in. Contour interval is 1 hPa. a) at lag 0, extrema in PC1 leading SLP by b) 1.5 years, c) 2 years, d) 3 years, e) 4 year, f) 5 years and g) 7 years. Shading indicates that the difference values are significant 95% confidence level.

Fig. 11 DJF composite difference of NCEP heat flux referenced to NCEP heat flux PC1. (a) at year -1, (b) year 0, (c) year 1, (d) year 2, (e) year 3 and (f) year 5. Contour interval for heat flux is 15 Wm-2. Areas where positive (negative) values are statistically significant at the 95% level are dark (light) shaded.

Fig. 12 DJF composite difference of COADS heat flux referenced to COADS heat flux PC1. (a) at year 0, (b) year 1, (c) year 2, (d) year 3, (e) year 5 and (f) year 6. Contour interval for heat flux is 10 Wm-2. Areas where positive (negative) values are statistically significant at the 95% level are dark (light) shaded.

Fig. 13 DJF composite difference of model heat flux referenced to model heat flux PC1. (a) at year 0, (b) year 1, (c) year 2, (d) year 3, (e) year 6 and (f) year 7. Contour interval for heat flux is 15 Wm-2. Areas where positive (negative) values are statistically significant at the 95% level are dark (light) shaded.

Fig. 14 DJF composite difference of SST, except (b) for MAM, by Smith et al. (1996) referenced to NCEP heat flux PC1. (a) at year 0, (b) MAM year 0, (c) year 1, (d) year 3, (e) year 6 and (f) year 7. Contour interval is 0.3C. Areas where positive (negative) values are statistically significant at the 95% level are dark (light) shaded.

Fig. 15 DJF composite difference of model SST referenced to model heat flux PC1. (a) at year 0, (b) year 1, (c) year 2, (d) year 3, (e) year 6 and (e) year 7. Contour interval for heat flux is 0.3 C. Areas where positive (negative) values are statistically significant at the 95% level are dark (light) shaded.

Fig. 16: Composite difference of the average temperature in the top 1000 meters from the ocean model simulation at the extrema of the model heat flux PC1 for DJF (a) year 0, (b) year 1, (c) year 2, (d) year 3, (e) year 6, and (f) year 7. The contour interval is 0.2C. The values in the areas of dashed shading are statistically significant at the 95% level.

Fig. 17: Composite difference of the March mixed layer depth anomalies from the ocean model simulation at the extrema of the model heat flux PC1 for DJF (a) year 0, and (b) year 7. The contour interval is 100m. The values in the areas of dashed shading are statistically significant at the 95% level.

FIG 18. EOF1 (a) and EOF2 (b) of OHC (upper 1000 m average temperature) and the PC1 (c), PC2 (d). Contour interval in (a-b) 0.2 non-dim. units, PC's are in units of C.

TABLE captions

Table 1: Periodicities in the North American Tide Gauge data from SSA- and Fourier analysis
Fourier analysis periods determined from two 50% overlapping subsections with a Hamming window (8 degrees of freedom) when compared to red noise 95 % confidence level.

Table 2: Periodicities in the European Tide Gauge data from SSA- and Fourier analysis
Fourier analysis periods determined from two 50% overlapping subsections with a Hamming window (8 degrees of freedom) when compared to red noise 95 % confidence level.

Table 3: The cold and warm winters (DJF) based on the extrema of heat flux PC1 above one standard deviation
(NCEP and MODEL uses 40 years of data, COADS 48 years; monthly PC1 binned seasonally)

Table 4: The schematic of the coupled cycle

TABLE 2

EUROPEAN SIDE				
Tide gauge station, latitude and record length	SSA modes 1,2	SSA-modes 3,4	SSA-modes 5,6	Fourier analysis significant period
Bergen, 60N, 69 years	7.74%, 7.15%	4.17%, 3.86%	2.46%, 2.03	9 and 15 years
SSA period	> Window	7-8 years		
Aberdeen, 56N, 104 years	7.87%, 7.05%	2.86%, 2.86%	2.26%, 2.21%	11 years
SSA period	> Window	14 years		
North Shields, 55N, 102 years	5.76%, 5.60%	3.62%, 3.23%		7, 11, 17 years
SSA period	12 years	irregular		
Brest, 48N, 83 years	6.81%, 5.70%	5.69%, 4.95%	2.58%, 2.57%	> 18 years
SSA period	> 20 years	irregular		
Lagos, 37N, 84 years	6.05%, 5.85%	4.90%, 4.57%	3.68%, 3.32%	11-14 years
SSA period	> Window	10 years		
Tenerife, 28N, 63 years	10.8%, 10.4%	8.25%, 7.82%		10 years
SSA period	10 years	irregular		

TABLE 1

N. AMERICAN SIDE				
Tide gauge station, latitude and record length	SSA modes 1,2	SSA-modes 3,4	SSA-modes 5,6	Fourier analysis significant period
Portland, 43N, 84 years	13.9%, 11.0%	5.50%, 5.24%	4.69%, 3.11%	8 years
SSA period	> Window	7-8 years		
Boston, 42N, 75 years	15.2%, 11.1%	3.95%, 3.95%	2.87%, 2.83%	10-13 years
SSA period	> Window	14 years, irreg.		
New York, 40N, 103 years	4.90%, 4.41%	3.95%, 3.94%	3.60%, 3.14%	7-8 years
SSA period	> Window	4 years		
Atlantic City, 39N, 84 years	6.79%, 6.73%	5.46%, 5.05%		8, 14 years
SSA period	13-14 years	irregular		
Charleston, 32N, 74 years	7.08%, 7.01%	4.20%, 3.67%		12 years
SSA period	12 years	irregular		
Mayport, 30N, 67 years	7.49%, 6.88%	4.43%, 3.64%		11 years
SSA period	12 years	irregular		

TABLE 3

Extrema of heat flux PC1 above one standard deviation

COLD WINTERS (the year of January in DJF)

NCEP	COADS	MODEL
1959	1949	1957
1962	1950	1959
1972	1952	1961
1973	1954	1972
1974	1957	1973
1975	1972	1974
1982	1975	1975
1984	1984	1984
1989	1989	1986
1990	1990	1989
1991		1990
1994		
1997		

WARM WINTERS (the year of January in DJF)

NCEP	COADS	MODEL
1964	1955	1954
1966	1958	1955
1968	1960	1958
1969	1964	1960
1970	1966	1964
1977	1968	1966
1978	1969	1968
1979	1970	1969
1980	1977	1970
1981	1979	1971
1987	1985	1979
		1980
		1983

TABLE 4. Evolution of the oceanic and atmospheric circulation anomalies during a half cycle of the decadal mode

YEAR	ATM. PATTERN	HEAT FLUX	SSTA OHCA	OCEANIC DYN. + ADV.	MOC at 25N
-1 - 0	NAO+	heating in subtropics; cooling in subpolar g.	warm subtropics cold subpolar g.	deep convection in subpolar g.	strong
1 - 2	NAO+ decaying	heating in subtropics; cooling in subpolar g.	warm subtropics, warm mid-ocean, cold slope waters, cold subpolar g.	N-E advection and amplification of warm OHCA in subtr.; southward adv. of cold subpolar OHCA	maximum
3 - 5	WA+	cooling in mid-ocean; heating in subpolar g.	warm mid-ocean warm subpolar g.	N-E advection of warm OHCA; subpolar deep convection weakens	weakens
6-7	NAO-	cooling in in subtropics; heating in subpolar g.	cold subtropics warm subpolar g.	no deep convection in subpolar g.	weak

NAO+/- has a low/high near Iceland and a high/low in the subtropics, WA+ has a low centered at 35-45N; MOC stands for meridional overturning cell; g. denotes gyre. Slope waters occupy the coastal area off the eastern seaboard between New Foundland and Cape Hatteras.

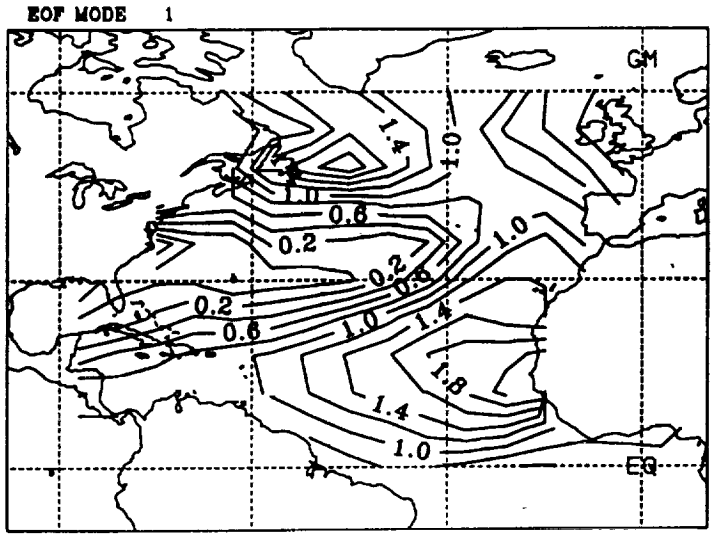
EOF MODE 1
GM
1.4
1.0
0.6
0.2
0.2
0.6
1.0
1.4
1.8
1.4
1.0
EQ

(a)

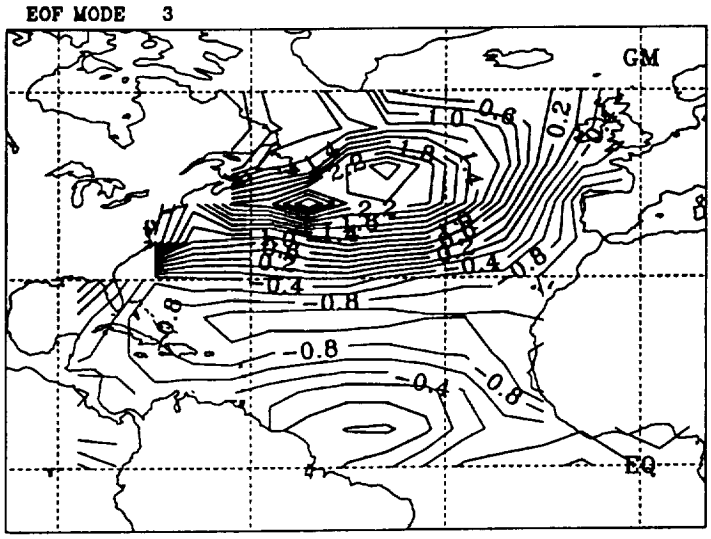
EOF MODE 3
GM
1.0
0.6
0.2
1.8
1.4
1.0
0.2
0.4
0.8
0.4
-0.8
-0.8
-0.4
-0.8
EQ

(b)

F1

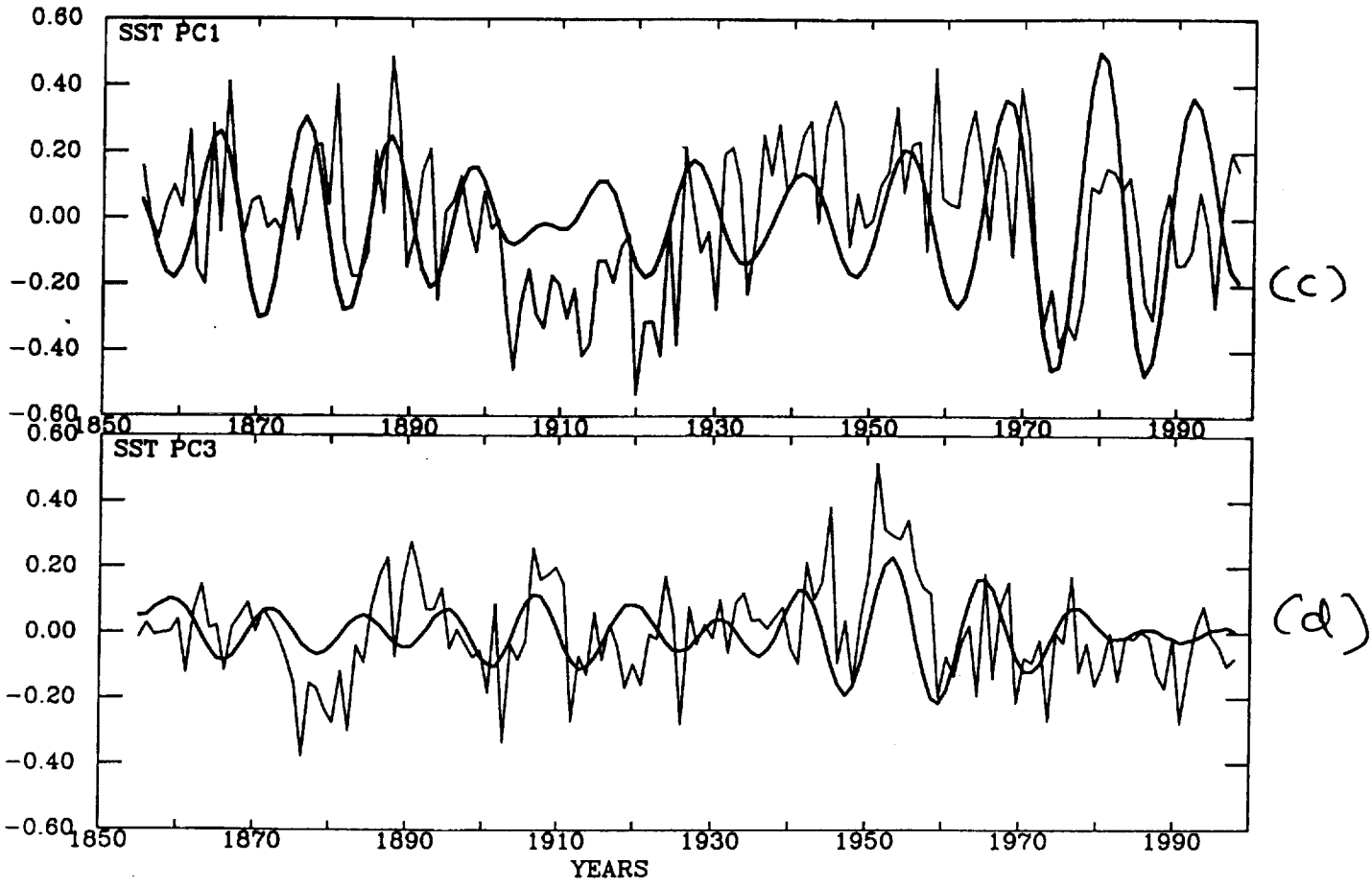
SST PC1
0.60
0.40
0.20
0.00
−0.20
−0.40
−0.60
1850
1870
1890
1910
1930
1950
1970
1990
(c)
SST PC3
0.60
0.40
0.20
0.00
−0.20
−0.40
−0.60
1850
1870
1890
1910
1930
1950
1970
1990
YEARS
(d)

F 1

Winter (JFM) SST anomalies SE of Florida and In the subpolar gyre (offset by 1C)

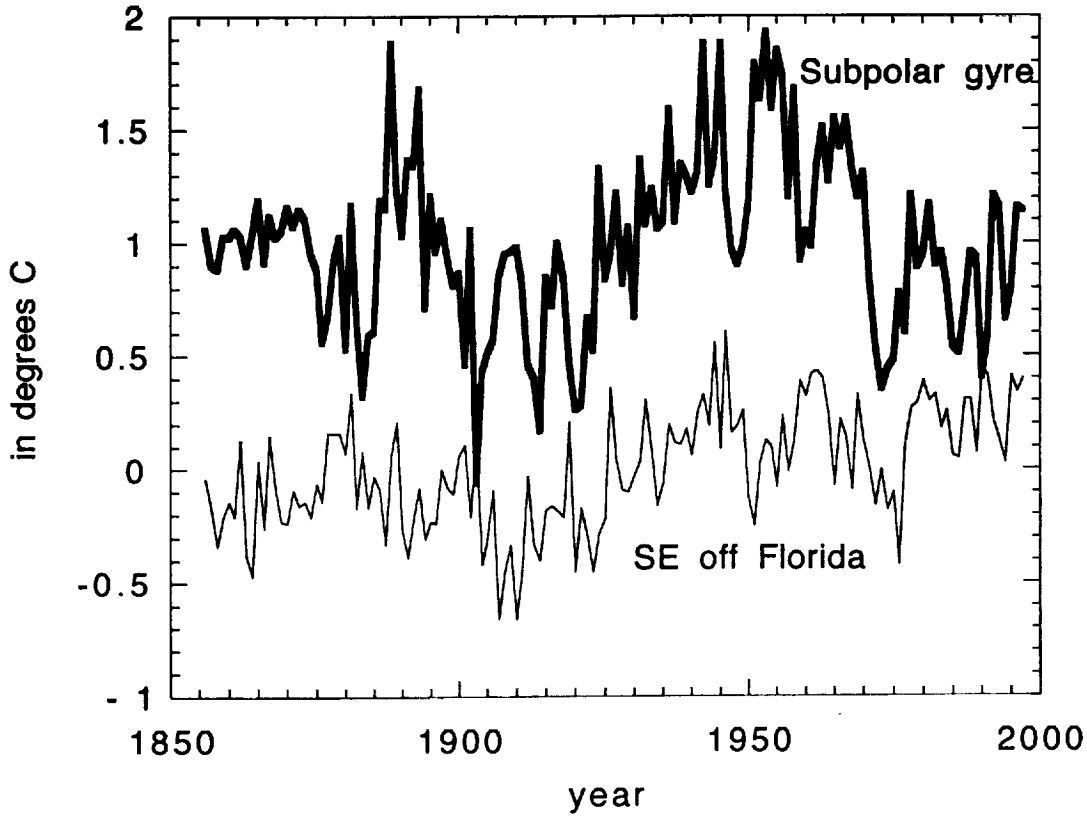

F 2a

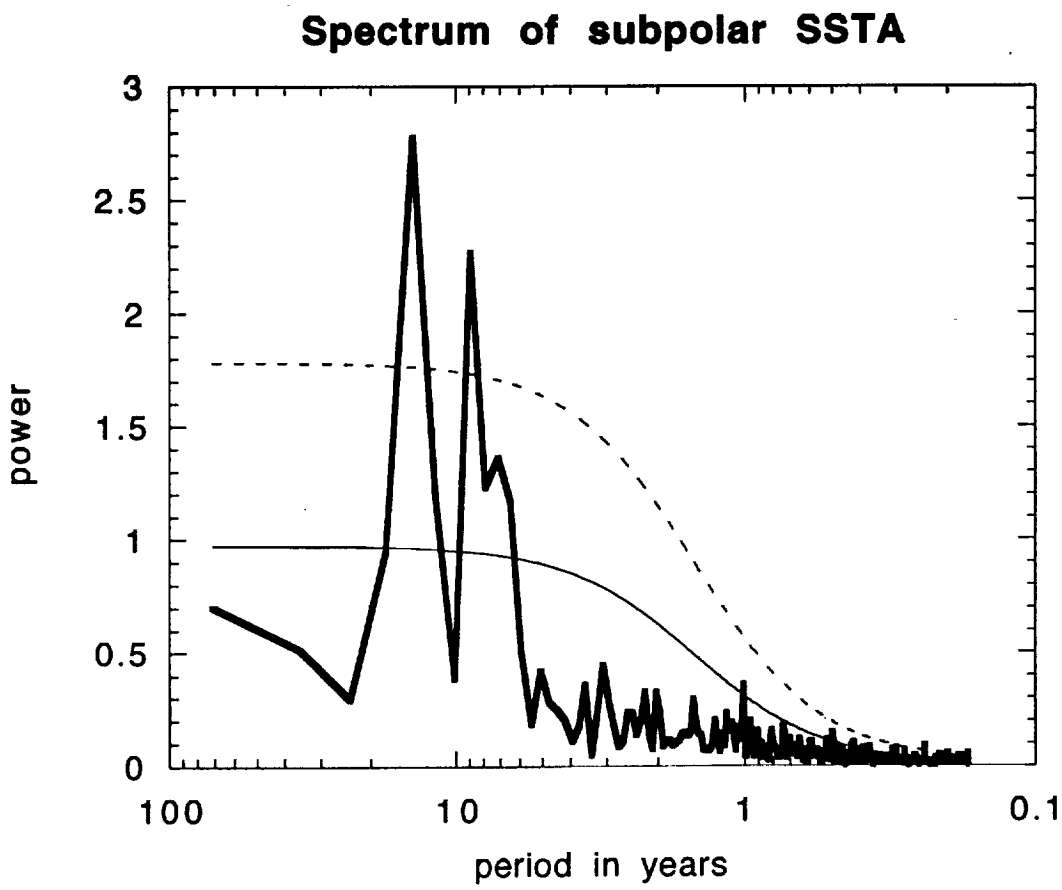
Spectrum of subpolar SSTA
power
3
2.5
2
1.5
1
0.5
0
100
10
1
0.1
period in years

F 2b

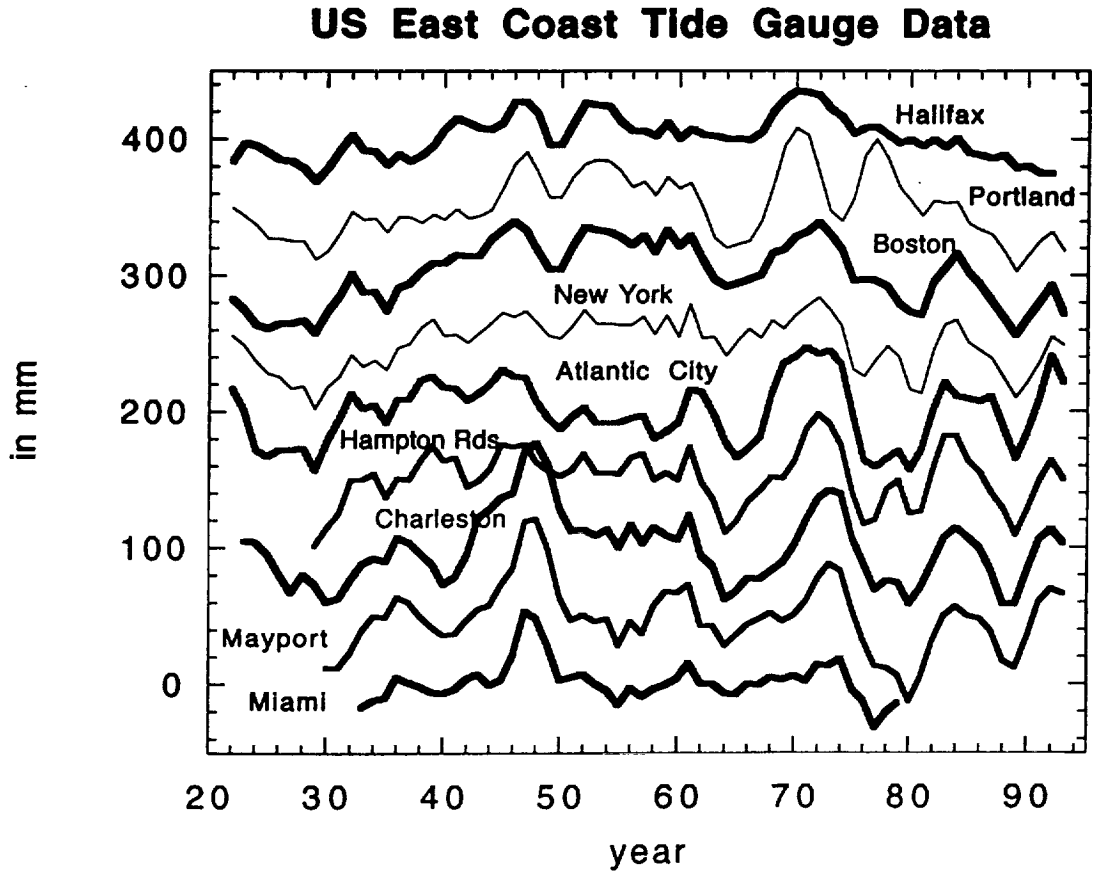
US East Coast Tide Gauge Data
Halifax
Portland
Boston
New York
Atlantic City
Hampton Rds
Charleston
Mayport
Miami
400
300
200
100
0
in mm
20
30
40
50
60
70
80
90
year

F 3

Detrended Charleston tide data, SSA 1&2 mode reconstruction and its 11-season running mean

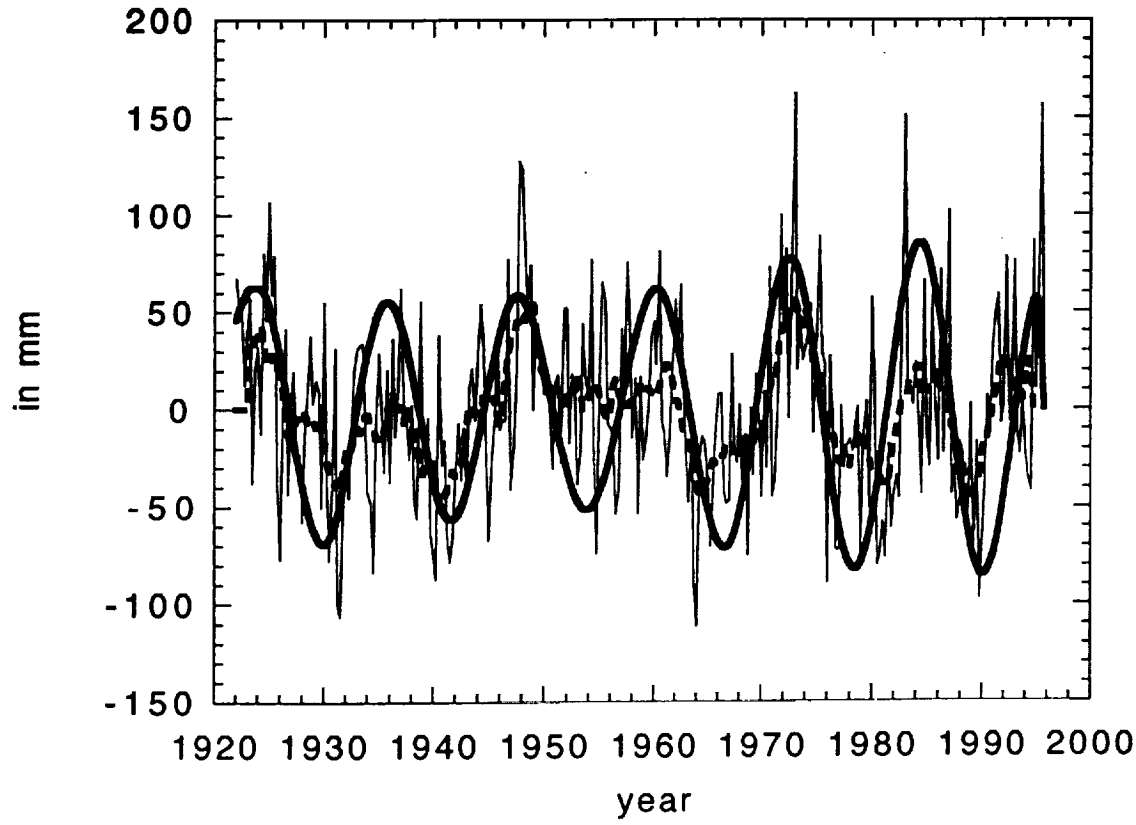

F4

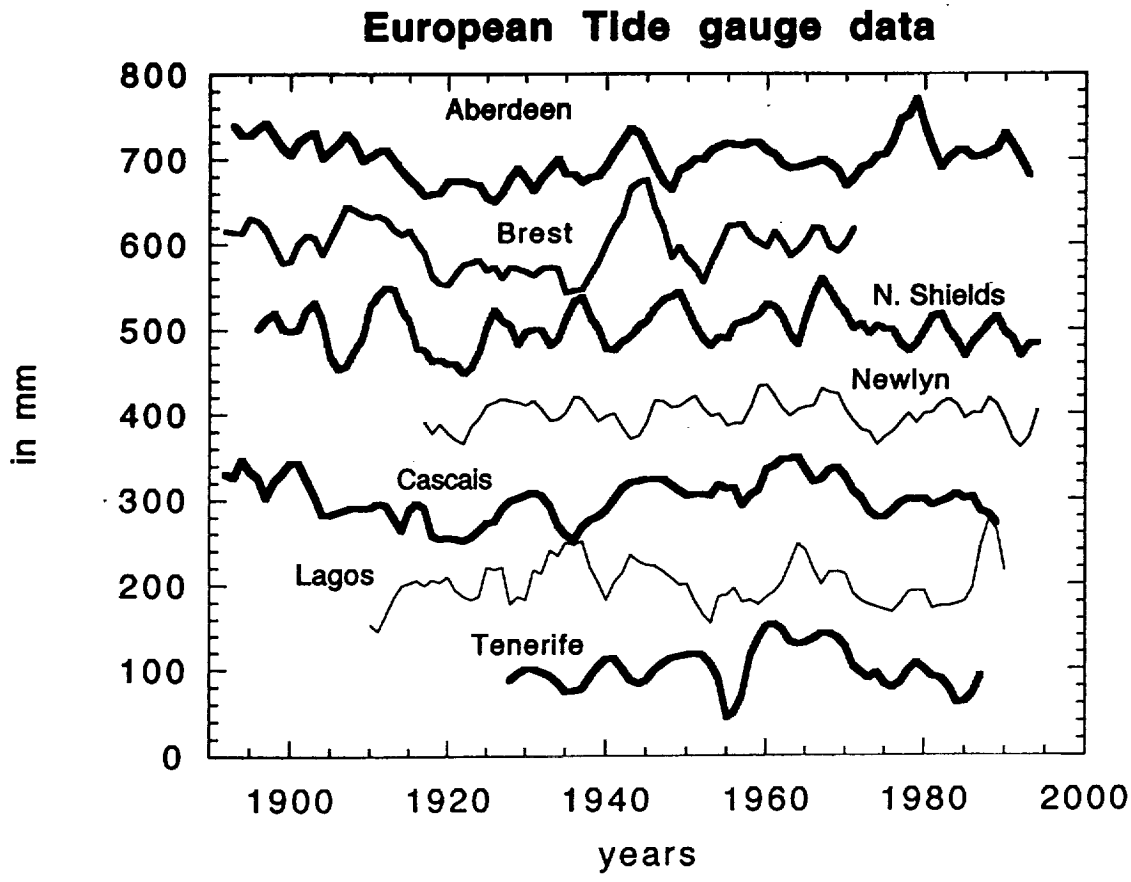
European Tide gauge data
800
700
600
500
400
300
200
100
0
in mm
Aberdeen
Brest
N. Shields
Newlyn
Cascais
Lagos
Tenerife
1900
1920
1940
1960
1980
2000
years

F5

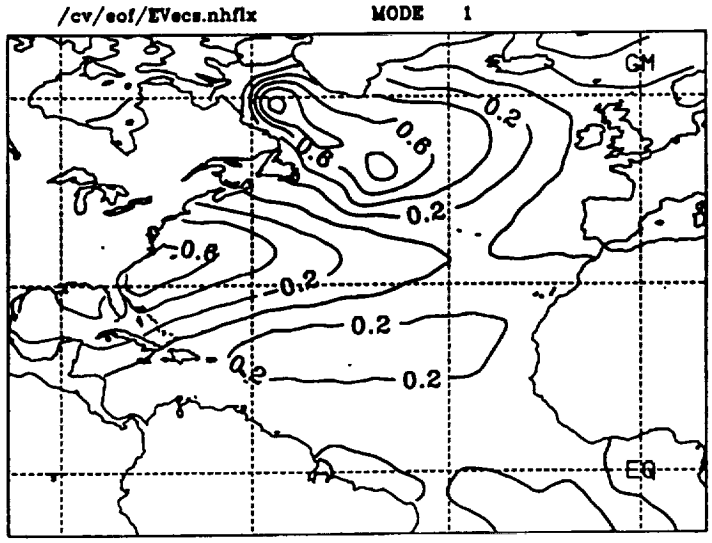
/cv/eof/EVecs.nhflx
MODE 1
GM
EQ
0.6
0.2
-0.6
-0.2

(a)

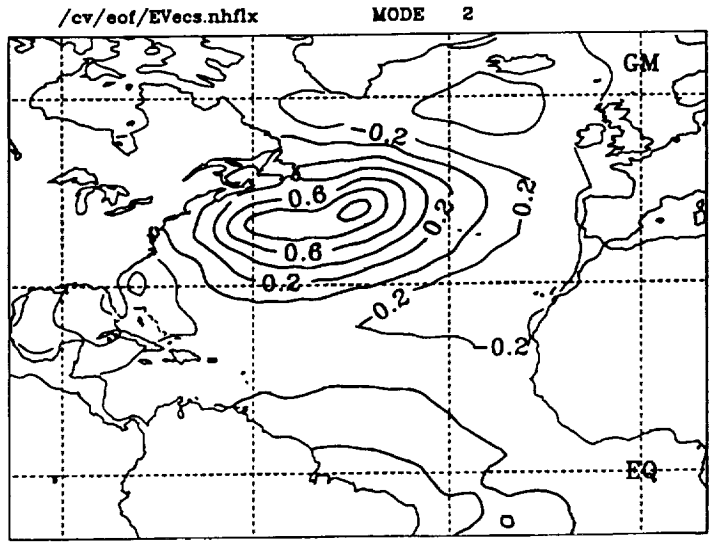
/cv/eof/EVecs.nhflx
MODE 2
GM
EQ
-0.2
0.6
0.2

(b)

F6

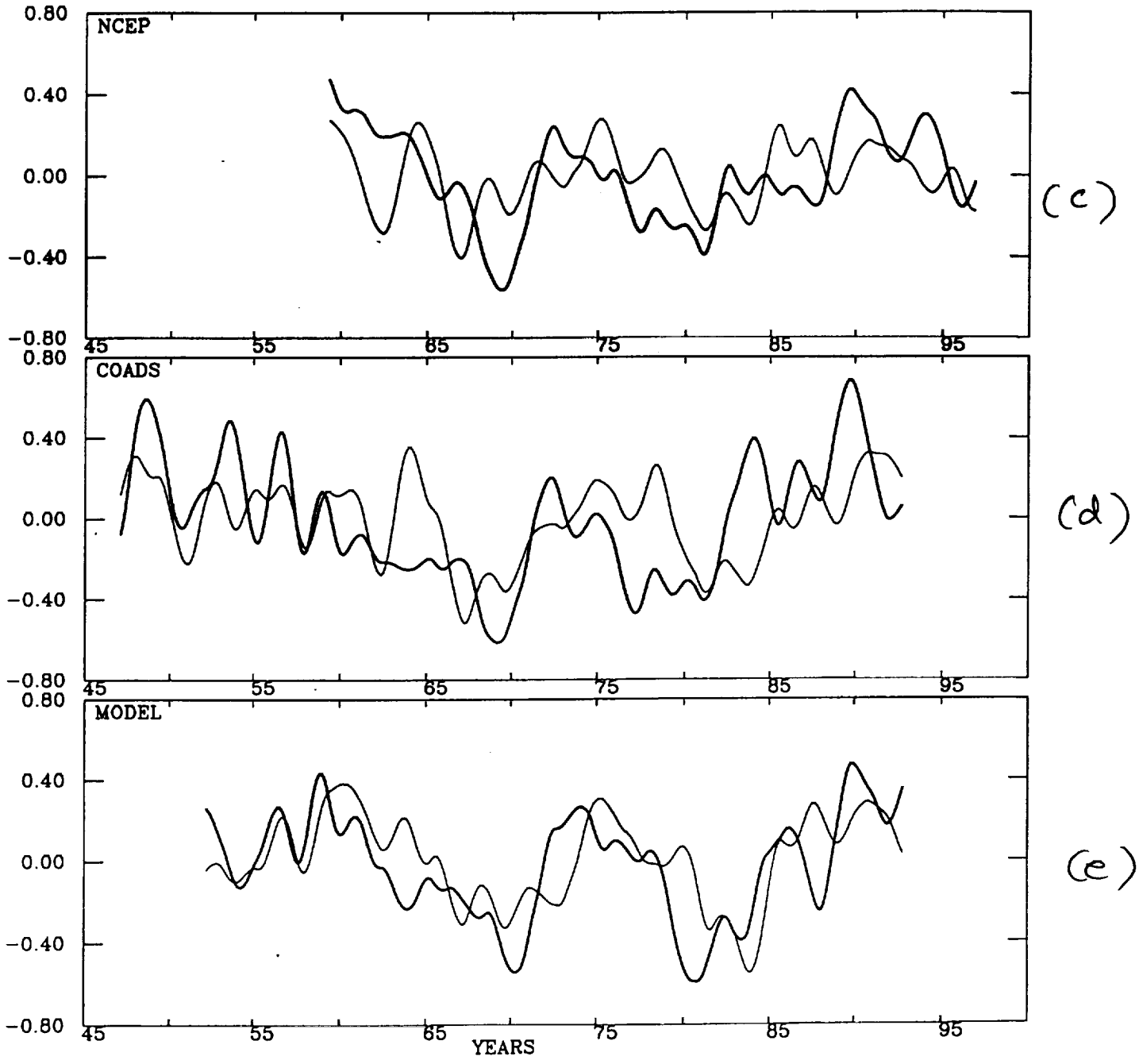

F6

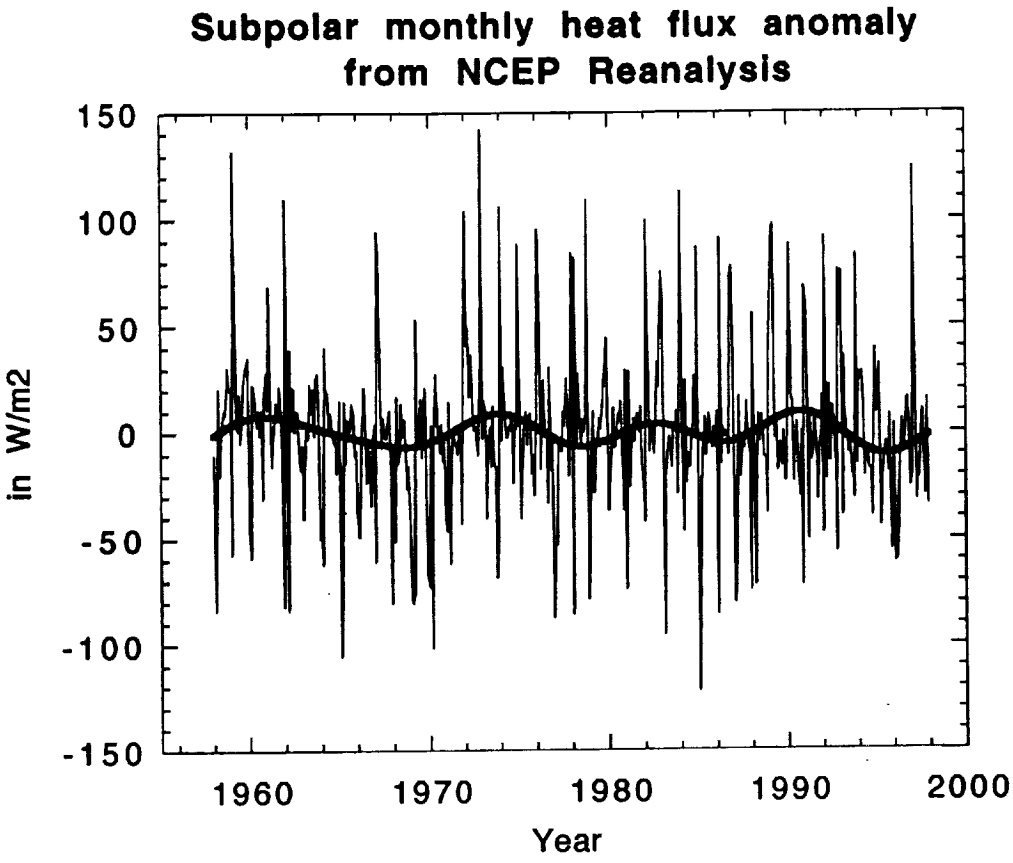
Subpolar monthly heat flux anomaly
from NCEP Reanalysis
150
100
50
0
-50
-100
-150
in W/m2
1960
1970
1980
1990
2000
Year

F7a

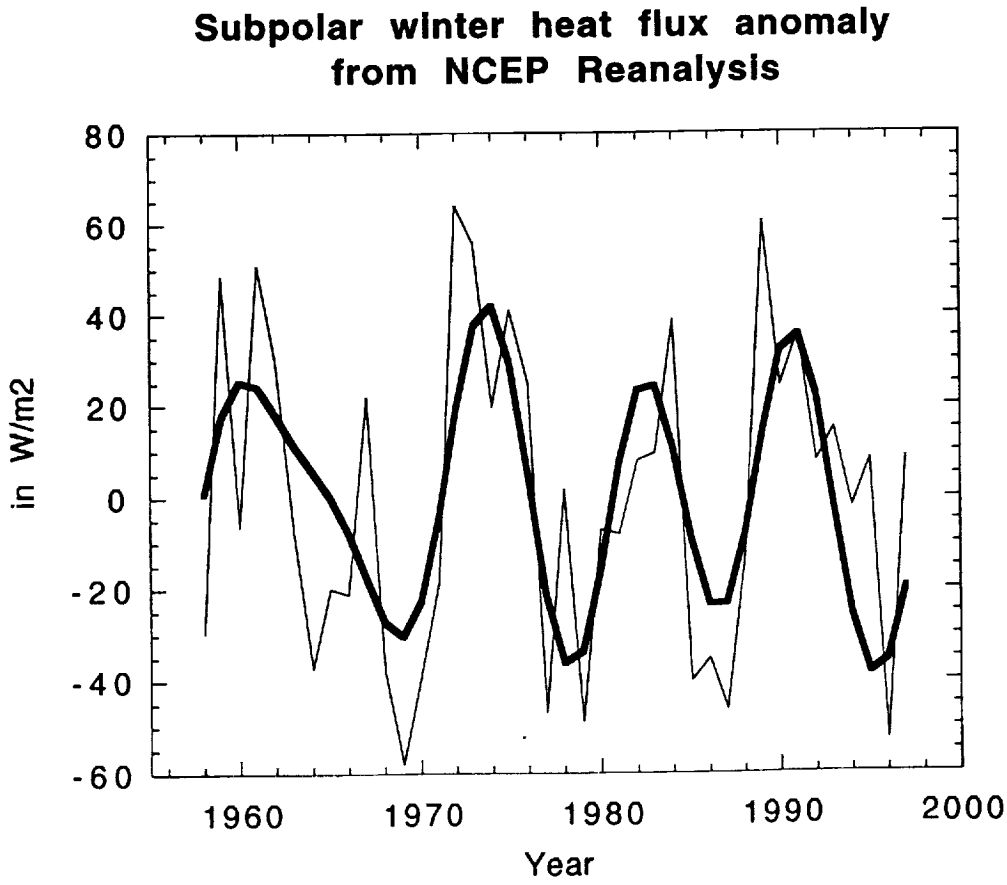
Subpolar winter heat flux anomaly
from NCEP Reanalysis
80
60
40
20
0
-20
-40
-60
in W/m2
1960
1970
1980
1990
2000
Year

F7b

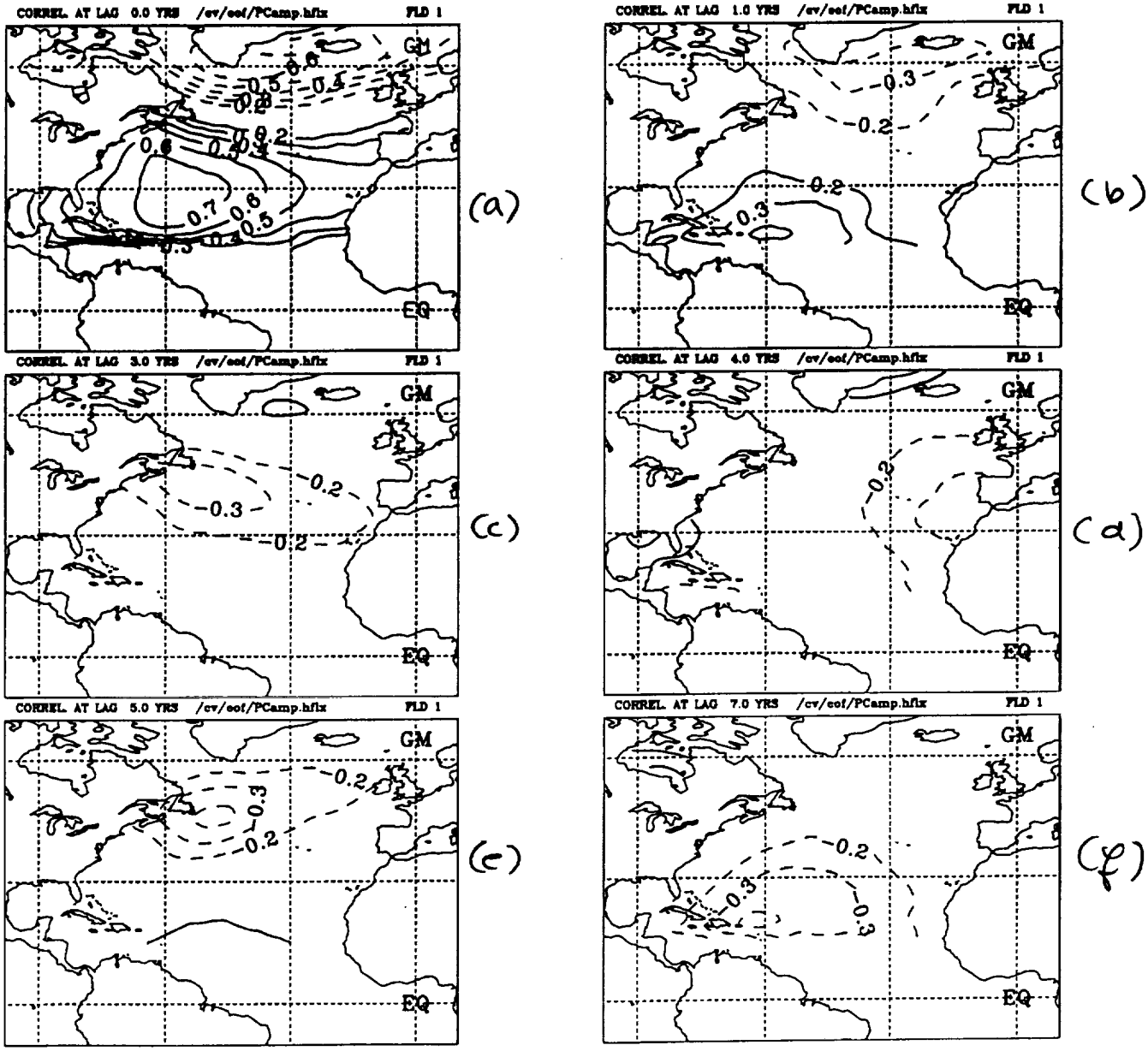
CORREL. AT LAG 0.0 YRS /cv/eof/PCamp.hflx FLD 1
GM
EQ
(a)
CORREL. AT LAG 1.0 YRS /cv/eof/PCamp.hflx FLD 1
GM
EQ
(b)
CORREL. AT LAG 3.0 YRS /cv/eof/PCamp.hflx FLD 1
GM
EQ
(c)
CORREL. AT LAG 4.0 YRS /cv/eof/PCamp.hflx FLD 1
GM
EQ
(d)
CORREL. AT LAG 5.0 YRS /cv/eof/PCamp.hflx FLD 1
GM
EQ
(e)
CORREL. AT LAG 7.0 YRS /cv/eof/PCamp.hflx FLD 1
GM
EQ
(f)

F8

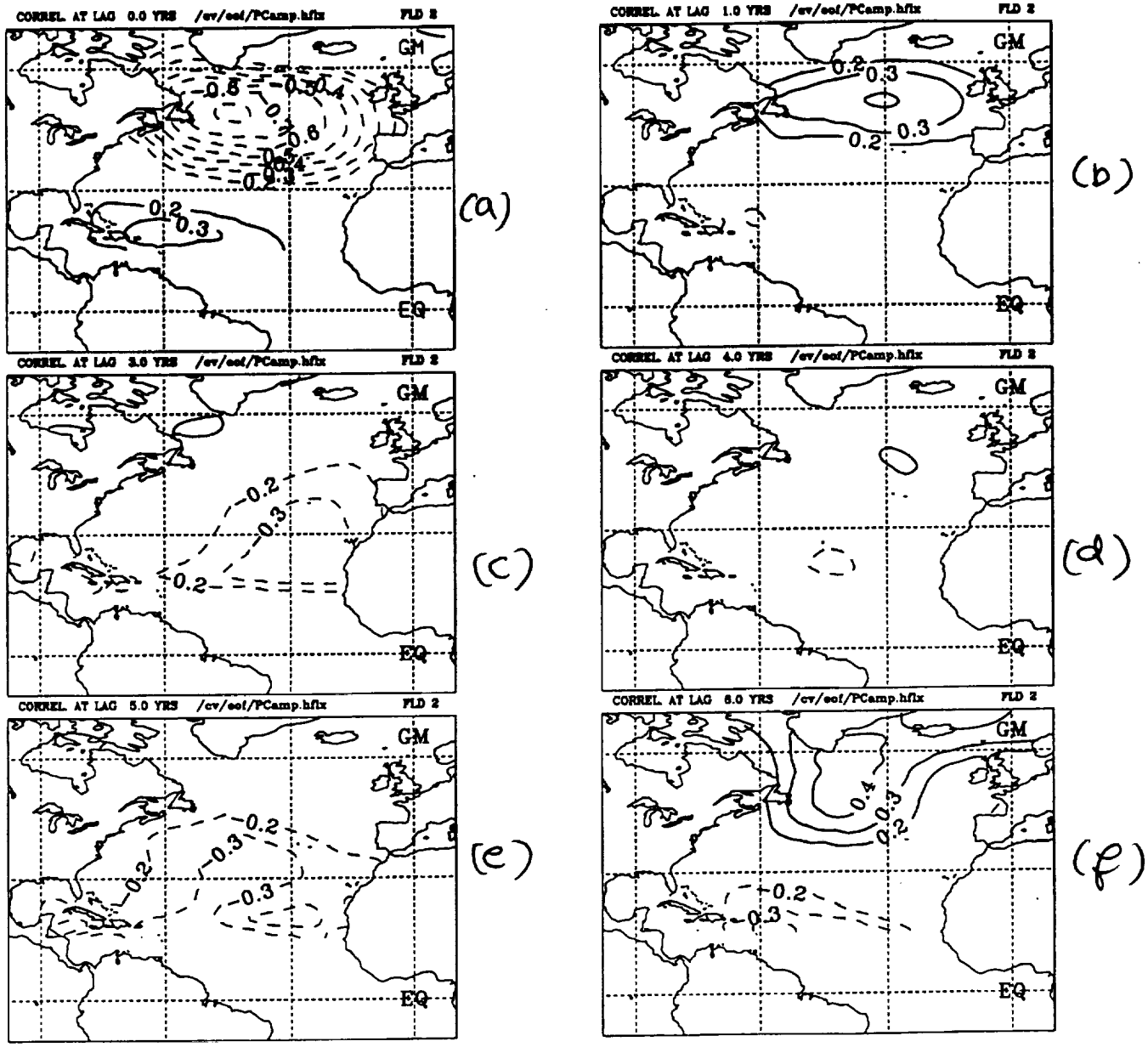
CORREL AT LAG 0.0 YRS /cv/eof/PCamp.hflx FLD 2
GM
EQ
-0.6
-0.5
-0.4
0
0.6
0.5
0.4
0.3
0.2
0.3
(a)
CORREL AT LAG 1.0 YRS /cv/eof/PCamp.hflx FLD 2
GM
EQ
0.2
0.3
0.2
0.3
(b)
CORREL AT LAG 3.0 YRS /cv/eof/PCamp.hflx FLD 2
GM
EQ
-0.2
-0.3
-0.2
(c)
CORREL AT LAG 4.0 YRS /cv/eof/PCamp.hflx FLD 2
GM
EQ
(d)
CORREL AT LAG 5.0 YRS /cv/eof/PCamp.hflx FLD 2
GM
EQ
-0.2
-0.3
-0.2
-0.3
(e)
CORREL AT LAG 6.0 YRS /cv/eof/PCamp.hflx FLD 2
GM
EQ
0.4
0.3
0.2
-0.2
-0.3
(f)

Fg

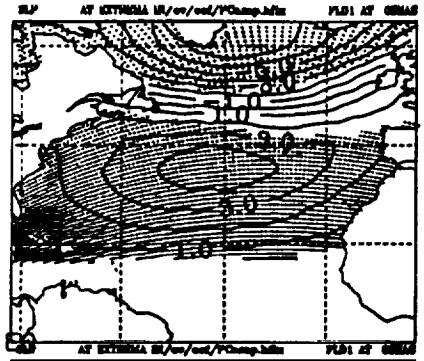

(a)

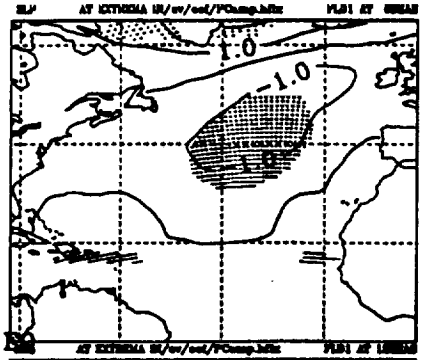

(b)

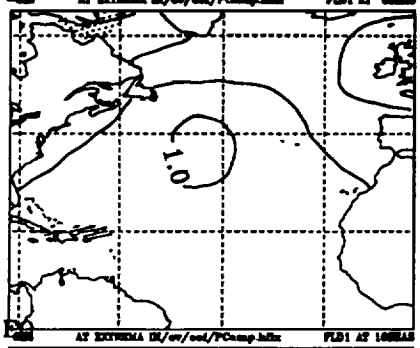

(c)

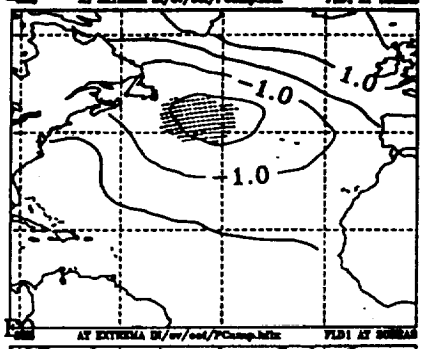

(d)

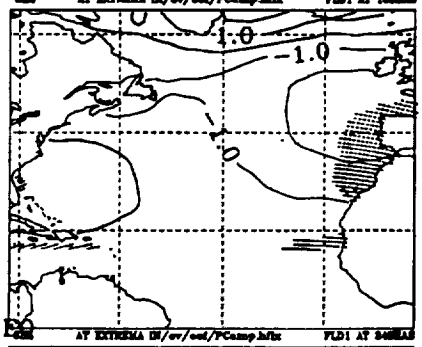

(e)

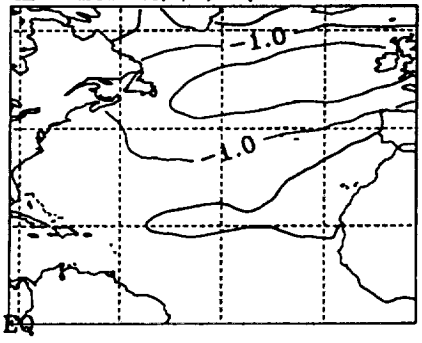

(f)

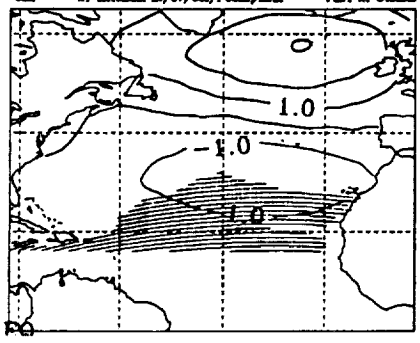

(g)

F10

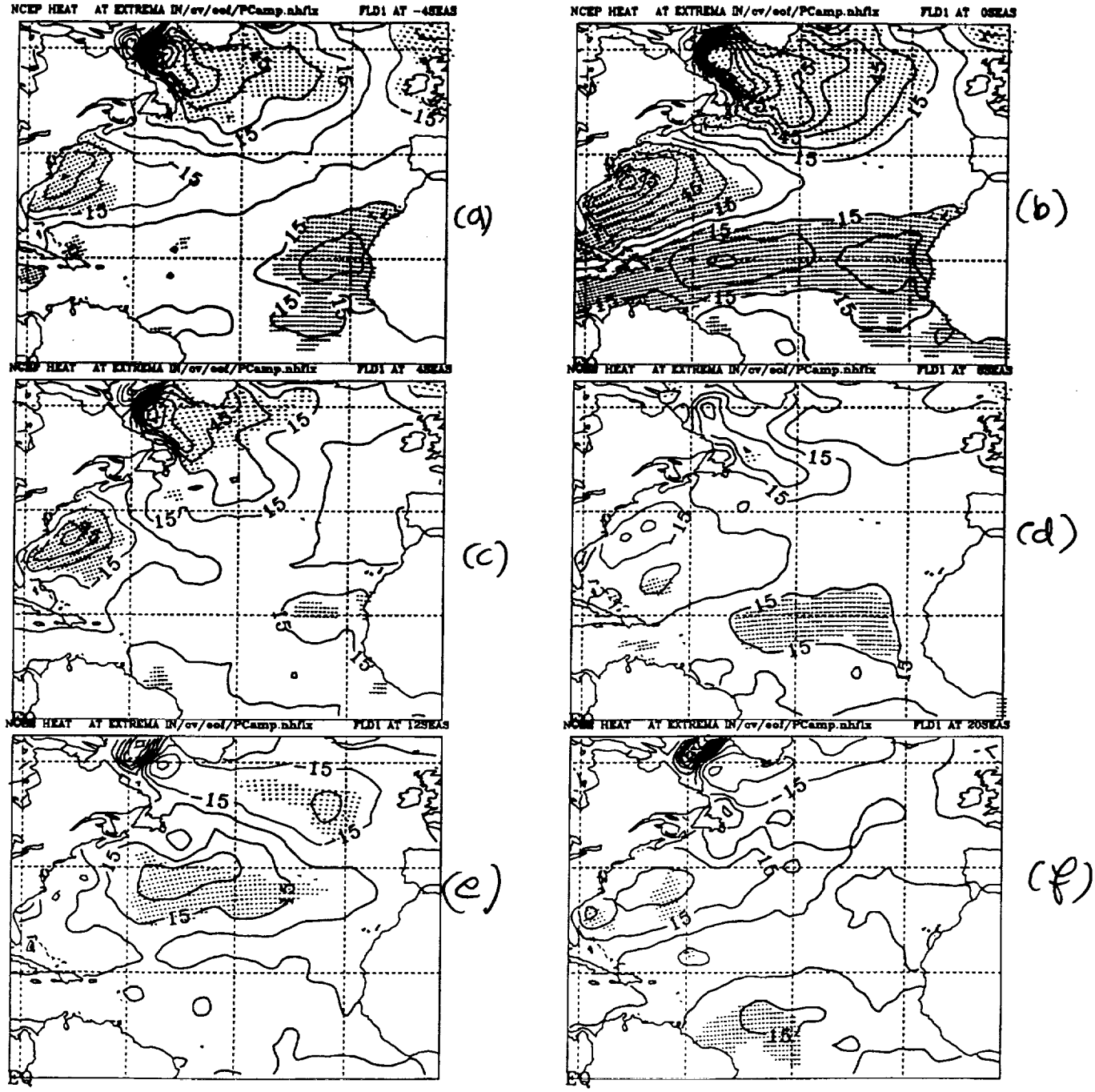
NCEP HEAT AT EXTREMA IN/cv/eof/PCamp.nhflx FLD1 AT -4SEAS
(a)
NCEP HEAT AT EXTREMA IN/cv/eof/PCamp.nhflx FLD1 AT 0SEAS
(b)
NCEP HEAT AT EXTREMA IN/cv/eof/PCamp.nhflx FLD1 AT 4SEAS
(c)
NCEP HEAT AT EXTREMA IN/cv/eof/PCamp.nhflx FLD1 AT 8SEAS
(d)
NCEP HEAT AT EXTREMA IN/cv/eof/PCamp.nhflx FLD1 AT 12SEAS
(e)
NCEP HEAT AT EXTREMA IN/cv/eof/PCamp.nhflx FLD1 AT 20SEAS
(f)

F 11

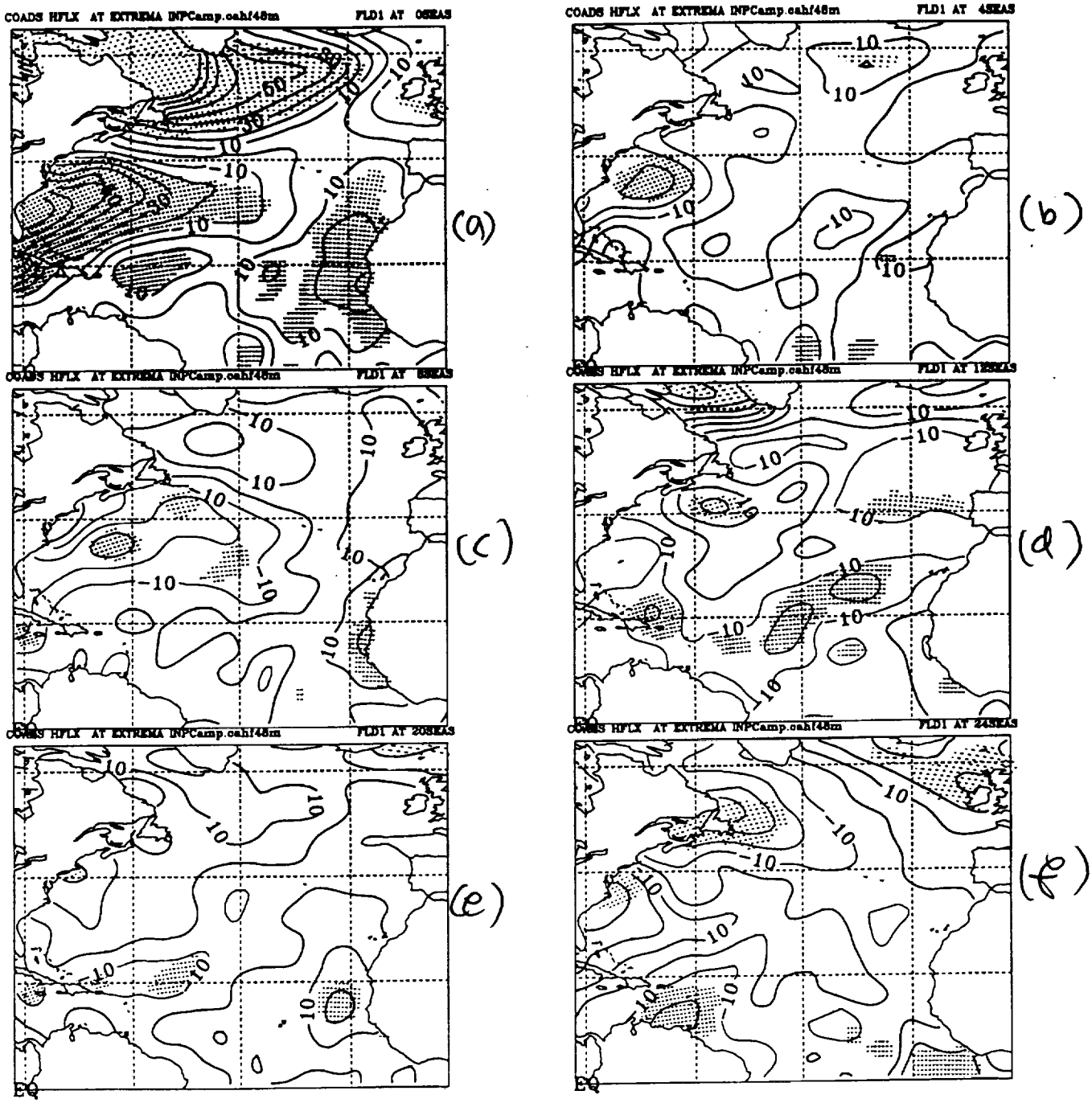
COADS HFLX AT EXTREMA INPCamp.cahf48m
FLD1 AT 0SEAS
(a)
COADS HFLX AT EXTREMA INPCamp.cahf48m
FLD1 AT 4SEAS
(b)
COADS HFLX AT EXTREMA INPCamp.cahf48m
FLD1 AT 8SEAS
(c)
COADS HFLX AT EXTREMA INPCamp.cahf48m
FLD1 AT 12SEAS
(d)
COADS HFLX AT EXTREMA INPCamp.cahf48m
FLD1 AT 20SEAS
(e)
COADS HFLX AT EXTREMA INPCamp.cahf48m
FLD1 AT 24SEAS
(f)
EQ

F12

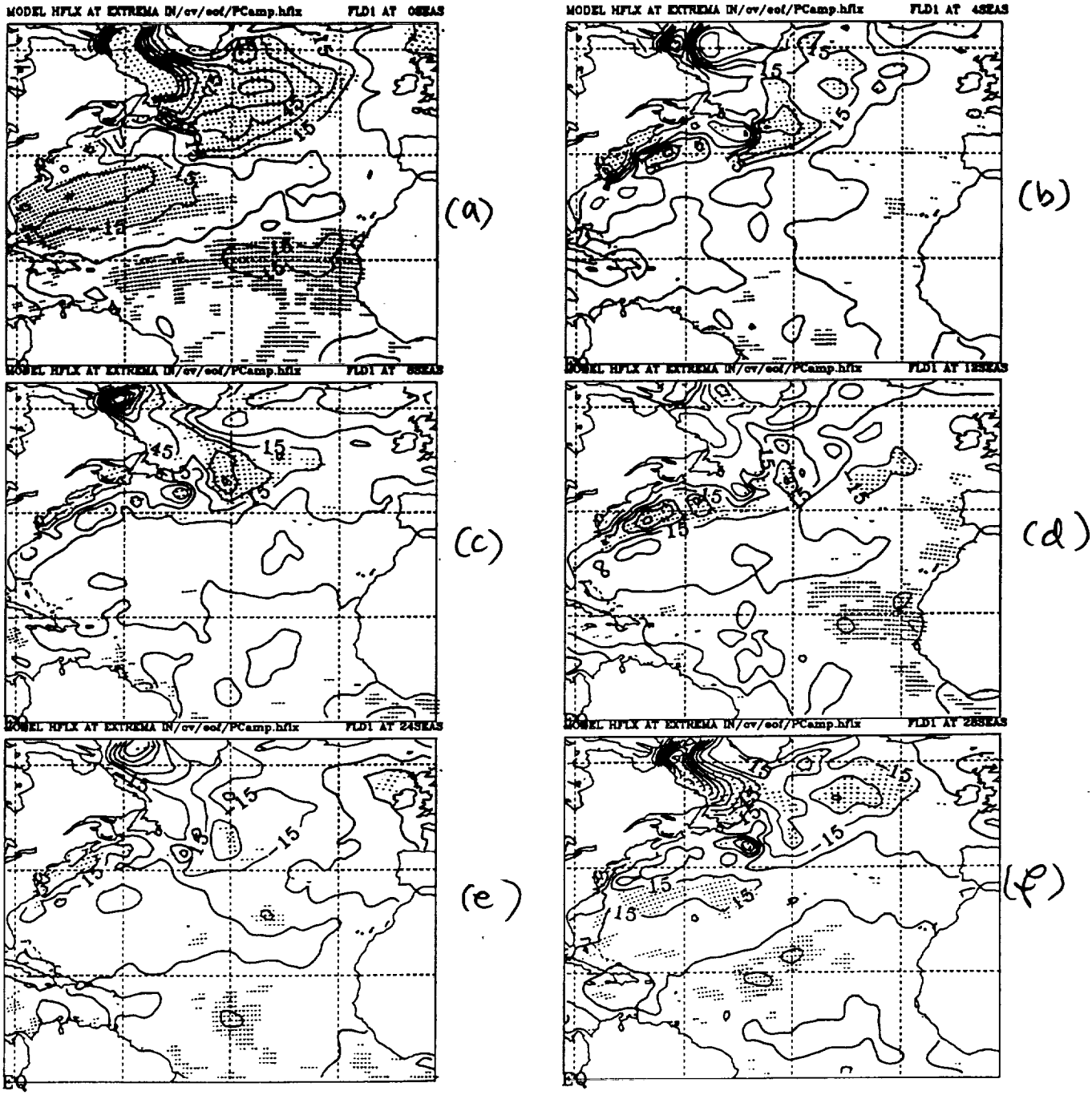
MODEL HFLX AT EXTREMA IN/cv/eof/PCamp.hflx FLD1 AT 0SEAS
(a)
MODEL HFLX AT EXTREMA IN/cv/eof/PCamp.hflx FLD1 AT 4SEAS
(b)
MODEL HFLX AT EXTREMA IN/cv/eof/PCamp.hflx FLD1 AT 8SEAS
(c)
MODEL HFLX AT EXTREMA IN/cv/eof/PCamp.hflx FLD1 AT 12SEAS
(d)
MODEL HFLX AT EXTREMA IN/cv/eof/PCamp.hflx FLD1 AT 24SEAS
(e)
MODEL HFLX AT EXTREMA IN/cv/eof/PCamp.hflx FLD1 AT 28SEAS
(f)
EQ

F13

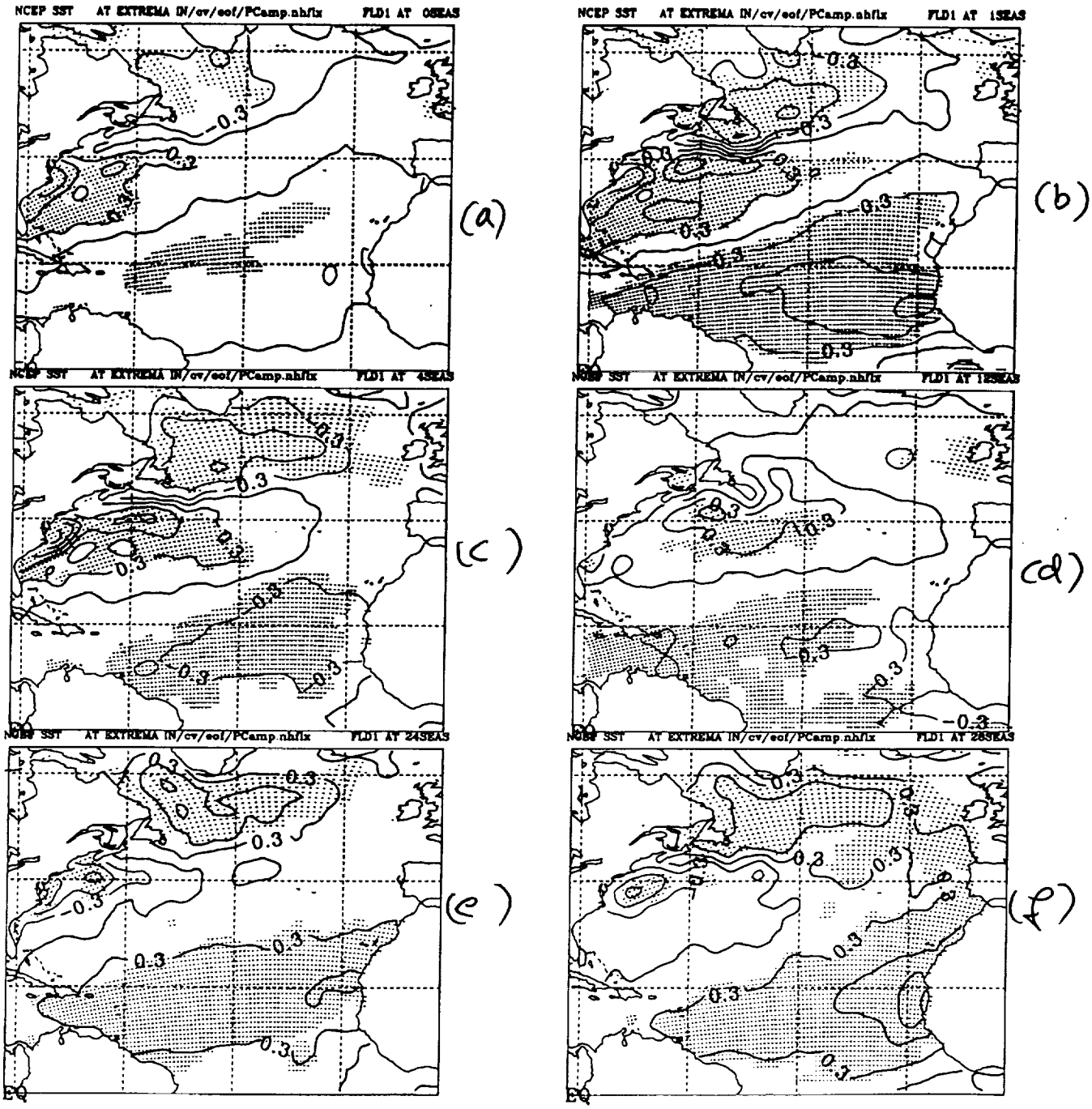
NCEP SST AT EXTREMA IN/cv/eof/PCamp.nhflx FLD1 AT 0SEAS
(a)
NCEP SST AT EXTREMA IN/cv/eof/PCamp.nhflx FLD1 AT 1SEAS
(b)
NCEP SST AT EXTREMA IN/cv/eof/PCamp.nhflx FLD1 AT 4SEAS
(c)
NCEP SST AT EXTREMA IN/cv/eof/PCamp.nhflx FLD1 AT 5SEAS
(d)
NCEP SST AT EXTREMA IN/cv/eof/PCamp.nhflx FLD1 AT 24SEAS
(e)
NCEP SST AT EXTREMA IN/cv/eof/PCamp.nhflx FLD1 AT 28SEAS
(f)

F14

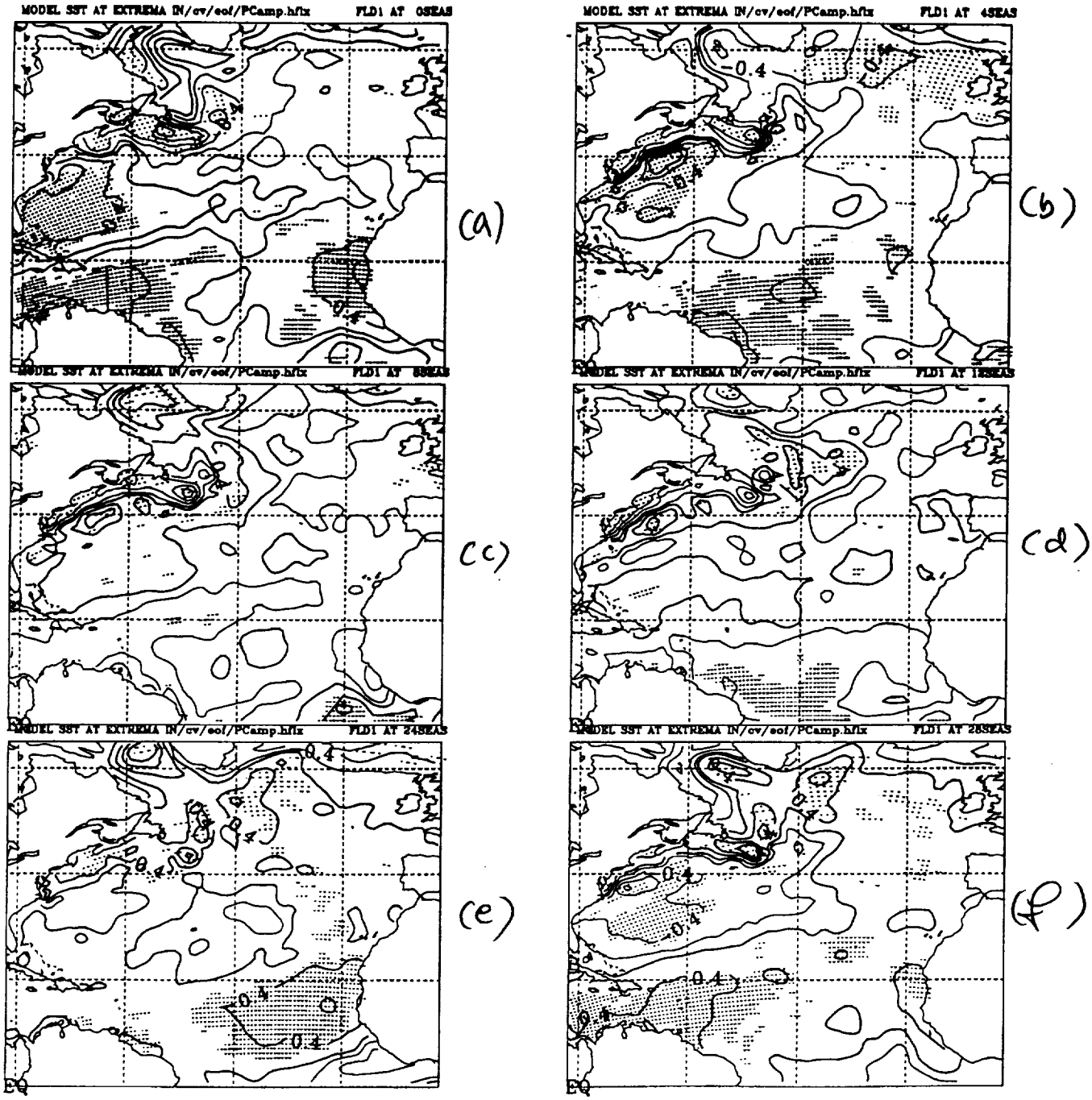
MODEL SST AT EXTREMA IN/cv/eof/PCamp.hfix FLD1 AT 0SEAS
MODEL SST AT EXTREMA IN/cv/eof/PCamp.hfix FLD1 AT 4SEAS
MODEL SST AT EXTREMA IN/cv/eof/PCamp.hfix FLD1 AT 8SEAS
MODEL SST AT EXTREMA IN/cv/eof/PCamp.hfix FLD1 AT 12SEAS
MODEL SST AT EXTREMA IN/cv/eof/PCamp.hfix FLD1 AT 24SEAS
MODEL SST AT EXTREMA IN/cv/eof/PCamp.hfix FLD1 AT 28SEAS
(a)
(b)
(c)
(d)
(e)
(f)
EQ

F15

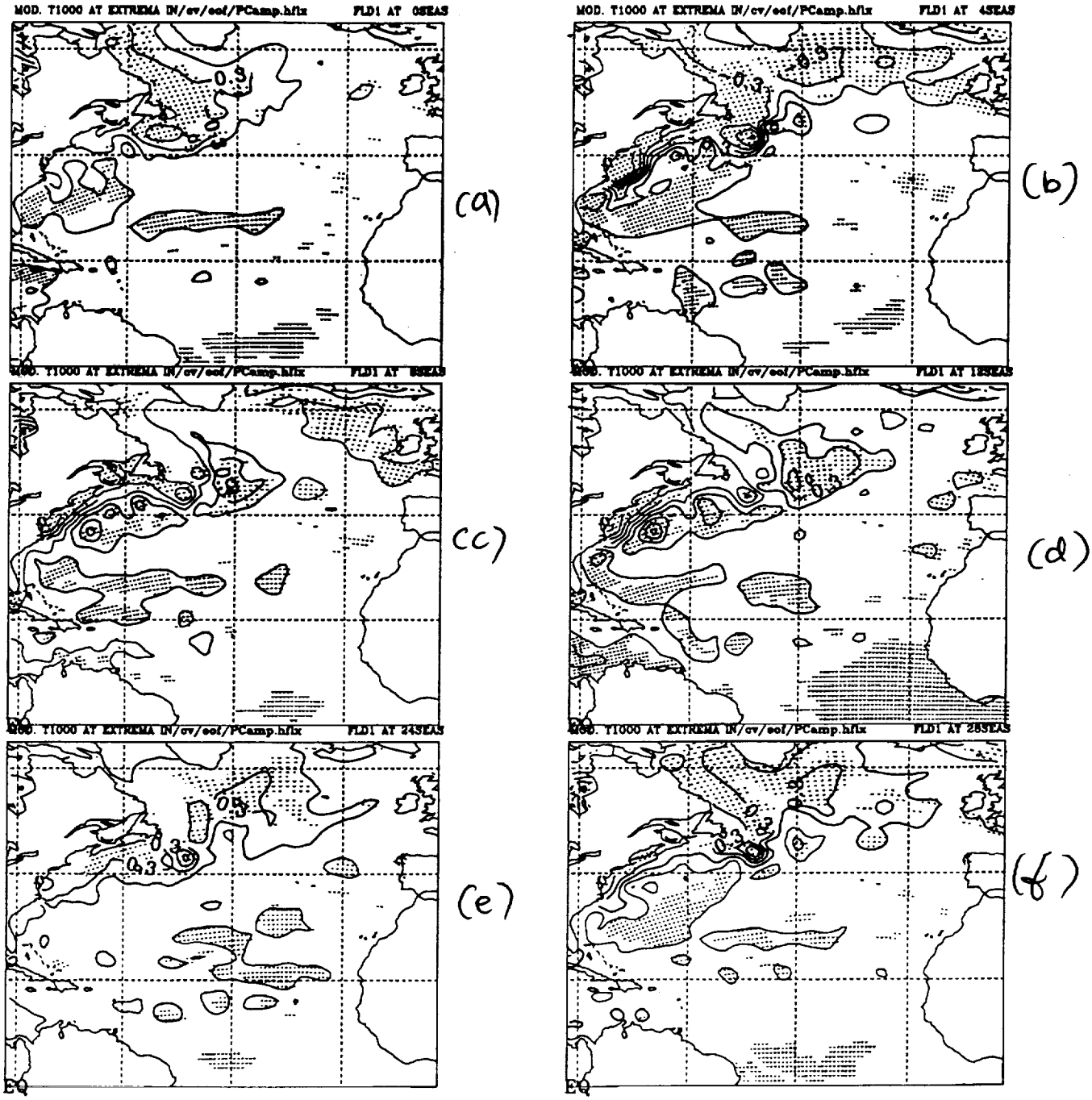
MOD. T1000 AT EXTREMA IN/cv/eof/PCamp.hflx FLD1 AT 0SEAS
MOD. T1000 AT EXTREMA IN/cv/eof/PCamp.hflx FLD1 AT 4SEAS
MOD. T1000 AT EXTREMA IN/cv/eof/PCamp.hflx FLD1 AT 8SEAS
MOD. T1000 AT EXTREMA IN/cv/eof/PCamp.hflx FLD1 AT 12SEAS
MOD. T1000 AT EXTREMA IN/cv/eof/PCamp.hflx FLD1 AT 24SEAS
MOD. T1000 AT EXTREMA IN/cv/eof/PCamp.hflx FLD1 AT 28SEAS
0.3
0.5
EQ
(a)
(b)
(c)
(d)
(e)
(f)

F16

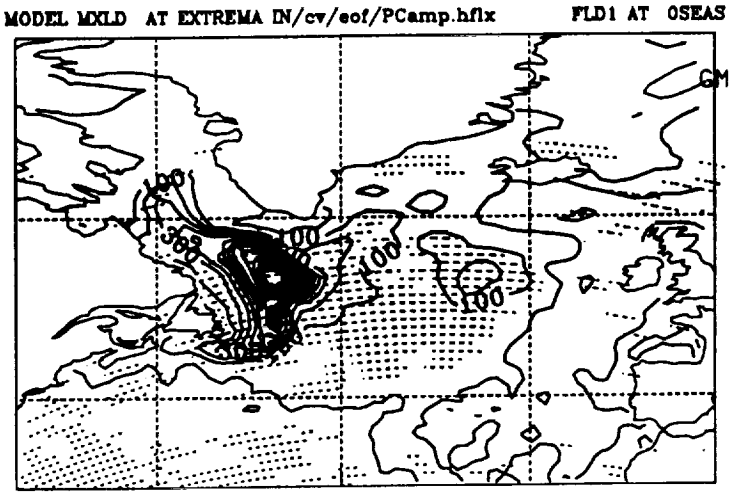
MODEL MXLD AT EXTREMA IN/cv/eof/PCamp.hflx
FLD1 AT 0SEAS
GM
100
100
100
100

(a)

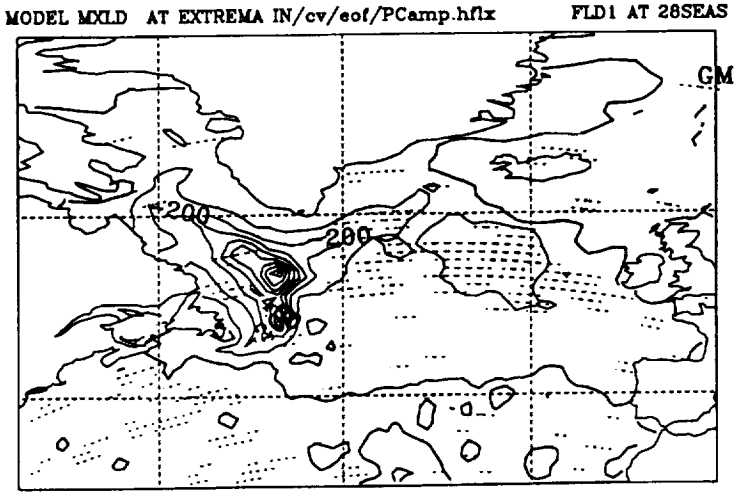
MODEL MXLD AT EXTREMA IN/cv/eof/PCamp.hflx
FLD1 AT 28SEAS
GM
200
200

(b)

F17

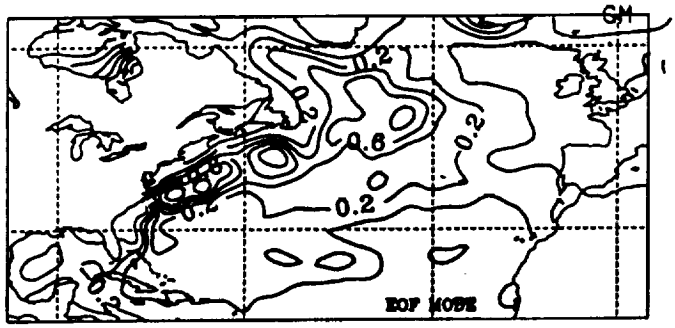
GM
0.2
0.6
0.2
EOF MODE

(a)

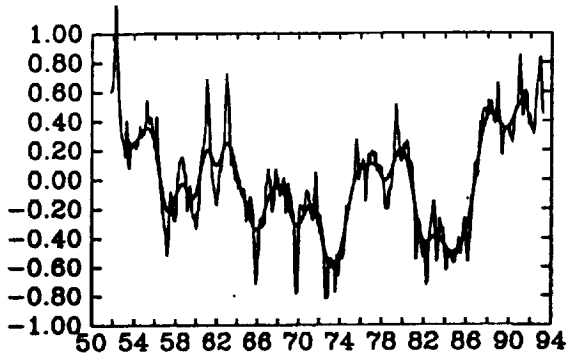
1.00
0.80
0.60
0.40
0.20
0.00
−0.20
−0.40
−0.60
−0.80
−1.00
50 54 58 62 66 70 74 78 82 86 90 94
YEARS

(c)

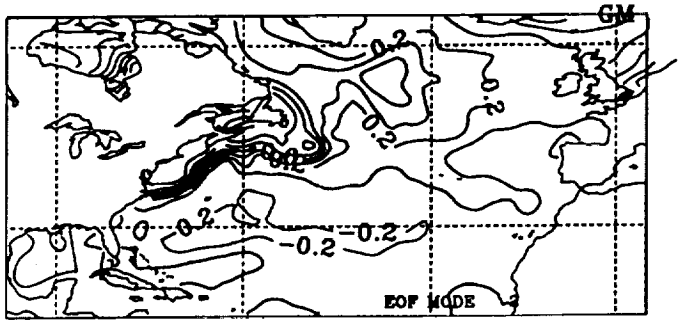
GM
0.2
0.2
0.2
0.2
0.2
-0.2
-0.2
EOF MODE

(b)

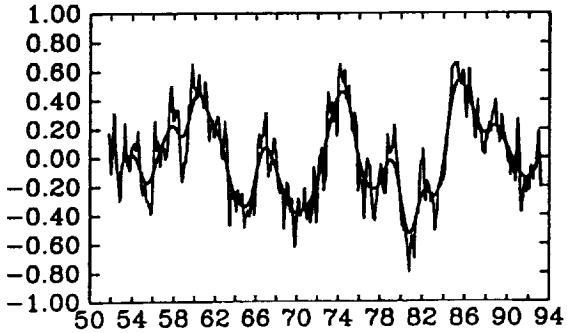
1.00
0.80
0.60
0.40
0.20
0.00
−0.20
−0.40
−0.60
−0.80
−1.00
50 54 58 62 66 70 74 78 82 86 90 94
YEARS

(d)

F18